



---

# THESIS BOOK

---

*Investigation on the potential of Hill Track Sites as solar fields  
for Concentrated Solar Powerplants incorporating Optical  
Efficiency as the primary parameter.*



**Investigation on the potential of Hill Track Sites as solar fields for  
Concentrated Solar Powerplants incorporating Optical Efficiency  
as the primary parameter.**

**MEE 490: PROJECT AND THESIS**

A thesis paper presented to the department of Mechanical Engineering, SUST,  
in partial fulfillment of the requirement for the Degree of Bachelor of Science  
in

Mechanical Engineering

by

Anwoy Talukder Ranjak [Reg No. 2018339045]  
Sayed Tanvir Ahmed [Reg No. 2017339050]

Under the supervision of

Tahmidul Haque Ruvo

Lecturer



Department of Mechanical Engineering  
Shahjalal University of Science and Technology  
Sylhet-3114, Bangladesh

February 2024

## **Declaration of authorship**

This is to certify that the work presented in this thesis entitled, "Investigation on the potential of Hill Track Sites as solar fields for Concentrated Solar Powerplants incorporating Optical Efficiency as the primary parameter.", is the outcome of the research carried out by Anwoy Talukder Ranjak and Sayed Tanvir Ahmed under the supervision of, Tahmidul Haque Ruvo, Lecturer, Department of Engineering, Shahjalal University of Science and Technology (SUST), Sylhet- 3114, Bangladesh.

It is also declared that neither this thesis nor any part thereof has been submitted anywhere else for the award of any degree, diploma, or other qualifications (except for publication).

Completed by -

---

Anwoy Talukder Ranjak  
Reg. No: 2018339045  
Department of Mechanical Engineering  
SUST

---

Sayed Tanvir Ahmed  
Reg. No: 2018339050  
Department of Mechanical Engineering  
SUST

Verified by -

20.03.24

---

Tahmidul Haque Ruvo  
Lecturer  
Department of Mechanical Engineering  
SUST

**Dedicated To**

Our beloved Parents and Teachers.

## **Acknowledgement**

First of all, we want to express our gratitude to the Almighty for providing us with the perseverance and fortitude to finish the task. We want to thank our thesis supervisors, AKM Ashikuzzaman, Lecturer, Department of Mechanical Engineering, SUST, and Tahmidul Haque Ruvo, Lecturer, Department of Mechanical Engineering, SUST, for all of their help, encouragement and patience. Their knowledge and keen criticism were extremely helpful in crafting this work.

We would also like to express our gratitude to the faculty and staff of the department for providing us with the tools, spaces, and academic support we needed to finish this project.

We also want to recognize the support and contributions of our family and friends, whose unflinching love and support have kept us going through this journey.

## **Abstract**

Renewable energy in the industrial sector is a key step in achieving low-carbon production systems. Concentrated Solar Power (CSP) technologies can be used to generate electricity by converting sunlight energy to power a turbine. Solar Power Tower (SPT) has become more developed and well-liked in recent years on a commercial scale, despite the fact that parabolic trough is still the most well-known and widely used CSP technology. In this study, the inclined barren surfaces of hillside areas are taken as solar fields which are named as Hillside Concentrated Solar Powerplant (HCSP) system. For this, three different barren hilly areas located at United States have been selected where the solar irradiation is moderately higher. A simple inclined plane V-shape layout with 5100 heliostats is simulated for optical efficiency in each of the locations for four days of a year and three times of a day. These simulation results show that the inclined rectangular array type layout provides greater optical efficiency at any of the three locations investigated than the optical efficiencies of the traditional horizontal plane functional layouts. Two real sites have been selected afterwards in the best performing location to plot an exact coordinate system and simulate the most optimum layout for those sites and the results are found in favor of the optimized layout which depicts that these optimized layouts result almost 20% higher optical efficiency than traditional horizontal plane functional layouts.

## Table of Contents

Declaration of authorship	i
Dedicated To	ii
Acknowledgement	iii
Abstract	iv
List of Figures	ix
List of Tables	xi
Nomenclature	xii
<b>Chapter 1: Introduction</b>	<b>1</b>
1.1    Solar Power and Thermal Power potential	1
1.2    Solar Energy	1
1.3    Concentrated Solar Power technology.	2
1.3.1    Parabolic Trough Collector (PTC)	2
1.3.2    Linear Fresnel Reflector (LFR)	2
1.3.3    Parabolic Dish Systems (PDS)	3
1.3.4    Solar Power Tower (SPT)	3
1.4    Earth parameters	4
1.5    Solar field	5
1.6    Layouts of a CSP field	5
1.7    Heat Transfer Fluid (HTF)	7
1.7.1    Thermal Energy Storage (TES)	7
1.8    Optical Efficiency ( $\eta_o$ )	7
1.9    SolarPILOT	9
1.10    Scope of the Thesis	10

<b>Chapter 2: Literature Review</b>	<b>12</b>
2.1    Field layout	12
2.2    Heat Transfer Fluid	14
2.3    Simulation software	15
2.4    Motivation of the present investigation	15
<b>Chapter 3: Physical Modeling</b>	<b>16</b>
3.1    V-shape inclined plane	16
3.1.1    Locations and field parameters	17
3.2    Real hill surfaces	19
3.2.1    Field data and parameters	19
3.2.2    Modelling real inclined surfaces	20
3.2.3    Optimum layout for Site 1	20
3.2.4    Optimum layout for Site 2	23
<b>Chapter 4: Mathematical Modeling</b>	<b>26</b>
4.1    Solar flux simulation	26
4.2    Shadowing efficiency	27
4.3    Cosine efficiency	28
4.4    Image intercept factor	29
4.5    Single simulation point	31
4.6    Extraterrestrial radiation	31
<b>Chapter 5: Model Validation</b>	<b>32</b>
5.1    Study of Wagner and Wendelin	32
5.2    Study of Ashikuzzaman and Adnan	32

5.3	Generation of layout	33
5.4	Validation	34
<b>Chapter 6: Result and Discussion</b>		<b>35</b>
6.1	Potential of inclined V-shape	35
6.2	Location 1	35
6.2.1	Blocking Efficiency	35
6.2.2	Receiver Flux profile	37
6.3	Location 2	40
6.3.1	Blocking Efficiency	40
6.3.2	Receiver Flux profile	42
6.4	Location 3	44
6.4.1	Blocking Efficiency	44
6.4.2	Receiver Flux profile	46
6.5	Efficiency data analysis	48
6.5.1	Location 1	48
6.5.2	Location 2	49
6.5.3	Location 3	50
6.6	Optical Efficiency analysis of three locations	50
6.7	Location 1 outperforming other locations	51
6.8	Site evaluation	52
6.8.1	Blocking Efficiency at Site 1	52
6.8.2	Receiver Flux profile at Site 1	54
6.8.3	Individual efficiency analysis	56
6.8.4	Blocking Efficiency for Site 2	57

6.8.5	Receiver Flux profile for Site 2	59
6.8.6	Individual efficiency analysis for Site 2	60
6.9	Optical Efficiency analysis of two sites	61
6.10	Overall potential of the sites	62
<b>Chapter 7: Conclusion</b>		<b>63</b>
7.1	Concluding remarks	63
7.2	Limitations and future work	64
<b>References</b>		<b>65</b>

## List of Figures

Figure 1. 1.	Schematic of PTC.	2
Figure 1. 2.	Schematic of LFR.	3
Figure 1. 3.	Schematic of PDS.	3
Figure 1. 4.	Schematic of SPT.	4
Figure 1. 5.	Traditional CSP field layouts.	7
 Figure 2. 1.	Optimized field layout with weighted efficiency as the objective (color scale represents the annual weighted efficiency for every heliostat within the field), (a) Campo radial-staggered, (b) biomimetic spiral.	12
Figure 2. 2.	Optical efficiency of (a) hybrid 1, (b) hybrid 2, (c) hybrid 3, (d) hybrid 4 and (e) hybrid 5 on the summer solstice generated by Ashikuzzaman and Adnan.	14
 Figure 3. 1.	Configuration of (a) the proposed inclined surface layout, and (b) the flat surface layout.	16
Figure 3. 2.	Simplified generation of HCSP (a) V-shape layout for inclined hill surfaces, and (b) the array of heliostats (dots represent the heliostats in the field).	17
Figure 3. 3.	Direct Normal Irradiation Map of USA.	18
Figure 3. 4.	Suitable sites with north and south wing spread for (a) site 1 and (b) site 2.	20
Figure 3. 5.	Test Layouts for Site 1 (a) Test Layout 1, (b) Test Layout 2, (c) Test Layout 3, (d) Test Layout 4, (e) Test Layout 5, (f) Test Layout 6, (g) Test Layout 7 to find out the optimum layout for Site 1.	22
Figure 3. 6.	Test Layouts for Site 2 (a) Test Layout 1, (b) Test Layout 2, (c) Test Layout 3, (d) Test Layout 4, (e) Test Layout 5, (f) Test Layout 6, to find out the optimum layout for Site 2.	24
 Figure 4. 1.	Relation between heliostat, the sun, and the position of the image plane	26
Figure 4. 2.	Heliostat normal vector and interfering heliostat subject vector orientations (a) depicting zero loss, (b) having dot product value of zero and (c) with positive dot product.	28
Figure 4. 3.	Sun vector and Normal vector orientation in the morning (a) and at noon in (b) flat horizontal layouts and (c) H-CSP layout.	29
Figure 4. 4.	A typical subdivision generated by SolarPILOT in a typical circumferential coordinate having varying density in both radial and azimuthal dimensions.	30
 Figure 5. 1.	Generated radial staggered layout (a) similar to the Crescent Dunes, Tonopah; and the optical efficiency (b) at 10am, for four specific	

days of the year for both the original and the generated similar layout on SolarPILOT.	34
Figure 6. 1. The blocking efficiency of the layout at different time and dates of the year at Location 1.	37
Figure 6. 2. The receiver flux profile at different time and dates of the year at Location 1.	39
Figure 6. 3. The blocking efficiency of the layout at different time and dates of the year at Location 2.	41
Figure 6. 4. The receiver flux profile at different time and dates of the year at Location 2.	43
Figure 6. 5. The blocking efficiency of the layout at different time and dates of the year at Location 3.	45
Figure 6. 6. The receiver flux profile at different time and dates of the year at Location 3.	47
Figure 6. 7. Variation of optical efficiency with the variation of time and date at (a) Location 1, (b) Location 2, and (c) Location 3.	51
Figure 6. 8. Blocking efficiency of the layout at different time and dates of the year at Site 1.	54
Figure 6. 9. The receiver flux profile at different time and dates of the year at Site 1.	56
Figure 6. 10. Blocking efficiency of the layout at different time and dates of the year at Site 2.	58
Figure 6. 11. The receiver flux profile at different time and dates of the year at Site 2.	60
Figure 6.12 Optical efficiency throughout the year for selected sites.	61

## List of Tables

Table 3. 1.	Proposed field data and the location parameters from the SolarPILOT Database.	18
Table 3. 2.	Proposed field data for two sites in Location 1.	19
Table 3. 3.	Test Layout properties for Site 1.	22
Table 3. 4.	Test Layout properties for Site 2.	25
Table 5. 1.	Validation of the current study with the study of Wagner and Wendelin.	32
Table 6. 1.	Individual Efficiencies in Location 1 (Blue Canyon Ap, California, USA).	48
Table 6. 2.	Individual Efficiencies in Location 2 (Deer Valley Phoenix, Arizona, USA).	49
Table 6. 3.	Individual Efficiencies in Location 3 (Lufkin, Texas, USA).	50
Table 6. 4.	Individual Efficiencies in Site 1.	56
Table 6. 5.	Individual Efficiencies in Site 1.	61

## Nomenclature

### 1. Notations and Symbols

X	Position of heliostat along X axis (m)
Y	Position of heliostat along Y axis (m)
Z	Position of heliostat along Z axis (m)
2D	Two dimensional
3D	Three dimensional
$\theta$	Radial Angle
$\phi$	Inclination angle with XY plane
$\delta$	Declination angle or latitude
$H_i, H_j, A_{i,j}$	Hermite polynomials
$\alpha_x, \alpha_y$	Standard deviation of the image distribution
$\mathbf{n}_j$	Heliostat normal vector
$\mathbf{i}_k$	Interfering heliostat subject vector
$n_{\text{cmax}}$	Number of computations
$\eta_o$	Optical efficiency (%)
$\eta_{\text{cosine}}$	Cosine efficiency (%)
$\eta_{\text{blocking}}$	Blocking efficiency (%)
$\eta_{\text{intercept}}$	Intercept efficiency (%)
$\eta_{\text{absorbtion}}$	Absorption efficiency (%)
r	Radial distance (m)
$\delta_0$	Extraterrestrial radiation intensity ( $\text{kW/m}^2$ )
u	Day number
$\Delta r$	Radial Extent
$\delta r$	Coordinates tolerance
$\Delta \beta$	Heliostat separation

### 2. Subscripts

$j$	Subject heliostat
$k$	Interfering heliostat
$o$	Optical
$i, j$	Individual heliostats

### **3. Abbreviations**

CSP	Concentrated Solar Power
HCSP	Hillside Concentrated Solar Power
PTC	Parabolic trough collector
HTF	heat transfer fluid
LFR	Linear Fresnel reflector
SPT	Solar power tower
DNI	Direct normal irradiance
LCOE	Levelized Cost of Electricity
CA	California
AZ	Arizona
TX	Texas
SAM	System Advisory Model

# **Chapter 1**

## **Introduction**

### **1.1 Solar Power and Thermal Power potential**

In recent decades, solar power has gained a lot of attention for producing quite a good amount of power compared to fossil fuel power plants with a positive impact on the environment. Over the past 20 years, the demand for solar energy has climbed by 20% to 25% [1]. Rather than this solar power can also be utilized to give heat to a range of industrial applications [2]. However, for being a diffuse energy source, solar power requires an efficient harness system. Solar photovoltaics and concentrated power plants are the most famous solar power harnessing processes due to their high efficiency. CSP has evolved in more than 20 countries ranging from 10MW to 500MW capacity [3]. An example can be Crescent Dunes solar thermal powerplant located at Tonopah, Nevada, USA, producing 500000 MWhr annually [4].

### **1.2 Solar Energy**

In the pursuit of sustainable and renewable energy sources, solar energy stands out as a beacon of promise. Harnessing the power of the sun, solar irradiance, direct normal irradiation, and overall solar radiation play pivotal roles in unlocking the potential of this clean and abundant energy.

- a. **Solar irradiance/insolation:** It is the rate at which solar energy falls on a unit area at the earth. The unit of measurement is ( $\text{W/m}^2$ ).
- b. **Solar radiation/ irradiation:** The amount of solar energy fallen for a specific period of time such as a day or year on a collector. Solar radiation is simply summation of solar irradiance over a period of time [5].
- c. **Direct normal irradiance (DNI):** The amount of solar radiation that is received by a unit surface area that is always held perpendicular or normal to the incident rays that is

coming in from the sun in a straight line at its current position. The DNI value is of particular interest in the study of CSP.

### 1.3 Concentrated Solar Power technology.

Concentrating solar power uses sunlight to generate electricity. The rays from the sun fall on a reflector or a series of reflectors which concentrate sunlight on a point which is then used to produce steam and is used in subsequent power generation. There are four types of CSP technologies available.

#### 1.3.1 Parabolic Trough Collector (PTC)

This type of CSP technology consists of a group of reflectors curved as parabola, which reflect sunlight in an absorber tube which is mounted on a group of parallel connected reflectors [6]. Figure 1.1 shows a PTC.

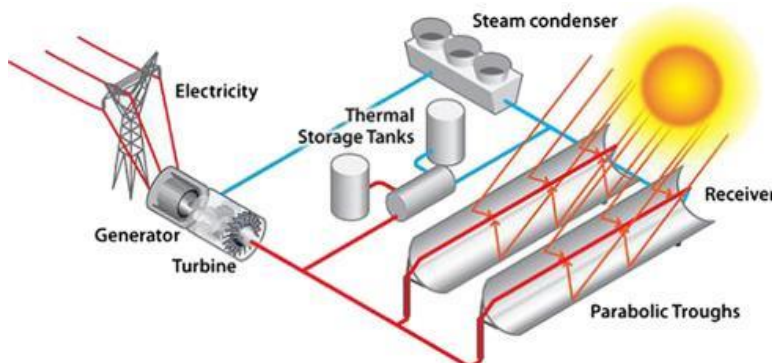


Figure 1. 1. Schematic of PTC [7]

#### 1.3.2 Linear Fresnel Reflector (LFR)

Figure 1.2 shows Linear Fresnel reflector using a series of flat or slightly curved mirrors to concentrate incoming solar beam on a downward facing receiver tube. As with the case with PTC, this type of CSP technology uses line focusing of incident sunlight.

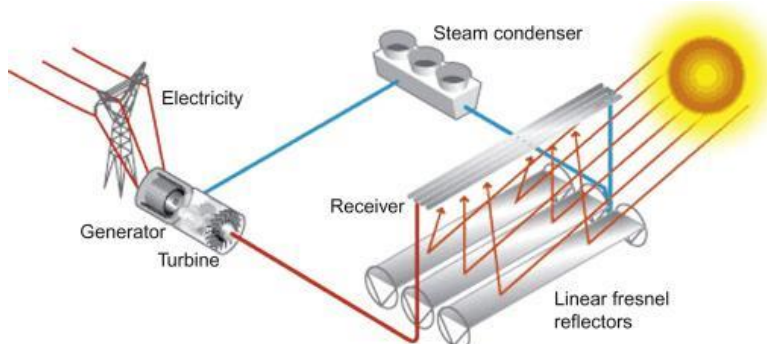


Figure 1. 2. Schematic of LFR [8].

### 1.3.3 Parabolic Dish Systems (PDS)

This system uses point concentration of incident rays rather than linear concentration. Figure 1.3 shows reflectors curved in parabolic shape concentrate solar radiation on a receiver mounted above it on the focal point.

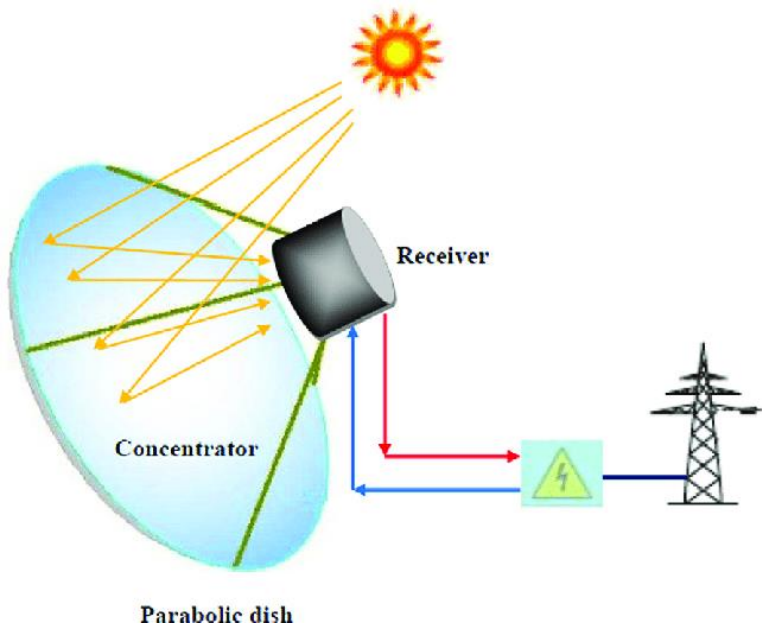


Figure 1. 3. Schematic of PDS [9].

### 1.3.4 Solar Power Tower (SPT)

Solar power tower, also known as central receiver system, which is the subjected technology of this study, shown in Figure 1.4 uses point concentration. A number of individual sun-tracking mirrors is used to concentrate incident sunlight on the top of a tower which is located centrally. A receiver consists of heat transfer fluid (HTF) which is

pumped up to the tower absorbs the heat. The heated fluid returns down the tower and then transfers heat to heat exchangers to a steam turbine in a thermal electrical power plant.

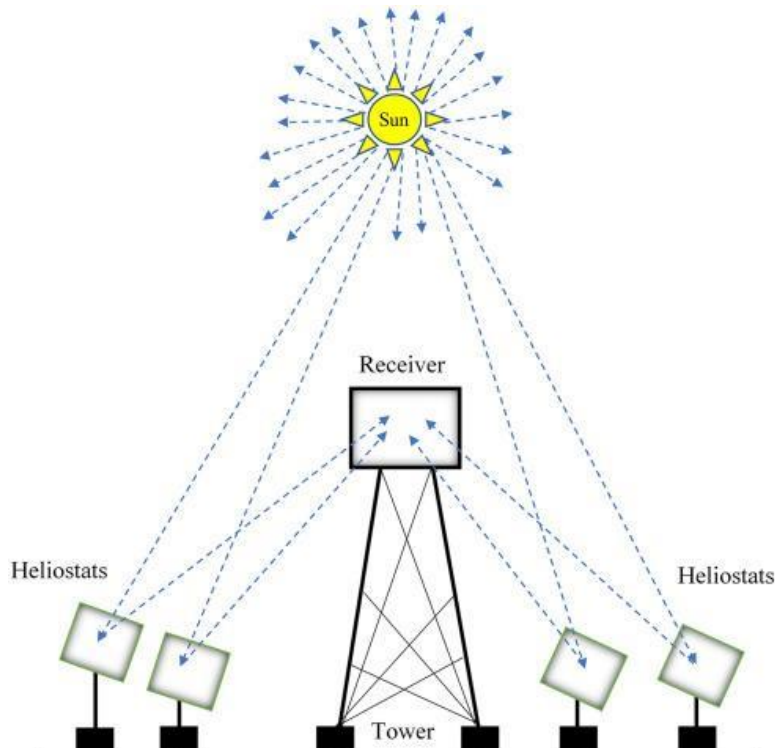


Figure 1. 4. Schematic of SPT [10].

Heat transfer fluid used in the system acts as thermal energy storage. Therefore, it can store thermal energy and dispatch it later when sunlight is not available. There are two types of thermal energy storage systems necessary for continuous electricity generation throughout the year, Short term, and long-term energy storage. Short term storage for using in nighttime or cloudy days while long term storage for using stored heat in summer for using in winter [11].

#### 1.4 Earth parameters

As we navigate the celestial dance between the Earth and the sun, several key parameters influence our experience of time and seasons. Solstices mark the extremes, with the summer solstice gracing us with the longest day on approximately 21<sup>st</sup> June and the winter solstice heralding the shortest day around 22<sup>nd</sup> December. Equinoxes, occurring around 21<sup>st</sup> March and 23<sup>rd</sup> September, bring a delicate balance, where day and night share equal prominence. Delving deeper into Earth's orientation, the solar elevation angle and solar

## Chapter 1

azimuth angle become crucial metrics, defining the angles that shape the sun's journey across our sky.

- a. **Solstices:** The longest day of the year known as summer solstice. Typically, 21st June. The shortest day of the year known as winter solstice. 22 December generally.
- b. **Equinoxes:** The two days of the year where day and night are equal. Spring and autumn equinox are typically 20 March and 23 September respectively.
- c. **Solar elevation angle:** It is the angle between the ray coming from the center of the sun, and a horizontal plane. Alternatively, it can be described in terms of the complement of the elevation angle which is known as solar zenith angle.
- d. **Solar azimuth angle:** The angle on the horizontal plane measured clockwise, from the north to the projection of the sun's central ray [12].

### 1.5 Solar field

The number of heliostats used in a horizontal plane consists of solar field. There are two types of solar field- first one is a North field; heliostats are placed only at the north of the solar tower. These layouts are used for small plants. And the second type is Surrounding field; The solar tower is surrounded by heliostats from every direction. This type of field is in use for medium and large power plants [13].

- a. **Heliostats:** The number of individually sun-tracking mirrors that is used to concentrate sunlight on a central tower is called heliostats. Heliostat numbers vary widely as the capacity of the power plant. They are slightly curved for higher flux density at the aim point.
- b. **Receiver:** To collect and absorb heat to transfer it to Heat transfer fluid (HTF), the receiver is located at the top of the tower. There are two types of receivers in use: external and cavity receiver.
- c. **Solar Tower:** A tower is located at the center of the solar field where all the reflected solar radiation is concentrated at the top of it where a receiver is placed [14].

### 1.6 Layouts of a CSP field

Field layout is mainly the arrangements of the heliostats in a CSP field. This parameter of a CSP plant is quite critical in the design phase of the plant. Layouts primarily have to utilize the land it is occupying to the fullest in terms of capturing solar irradiation and

## Chapter 1

reflect the irradiation to the central receiver. Many losses incorporating this process, resulting in some traditional layouts that can be easily formable and minimize much of the losses. Field layouts is seen to be influenced by patterns existing in nature. A few traditional layouts like radial staggered, corn field has been primary pick for a numerous study, which afterwards suggests a better layout or hybrid of some to conclude with a better efficiency or power output. For instance, Figure 1.5 shows radial staggered, biomimetic spiral and corn field layouts.

- a. **Radial Staggered Layout:** Mirrors are arranged in a radial pattern around a central tower. Staggering the mirrors helps to minimize shading and optimize sunlight collection. This layout allows for efficient use of land while maintaining a high level of sunlight concentration on the central receiver.
- b. **Biomimetic Spiral Layout:** Inspired by patterns found in nature, particularly the spiral arrangements seen in certain plant structures. This layout aims to maximize sunlight capture and concentration efficiency by mimicking the optimal arrangement observed in natural systems.
- c. **Cornfield Layout:** In this layout, heliostats are arranged in rows resembling the layout of a cornfield. The goal is to densely pack mirrors while maintaining optimal spacing to avoid shading. This layout is designed to balance efficiency with ease of maintenance and operation.

These layouts are part of the innovative approaches in CSP design, aiming to enhance energy capture, improve system efficiency, and make better use of available land. Each layout has its advantages and may be chosen based on factors such as the local climate, land availability, and the specific design goals of the CSP plant.

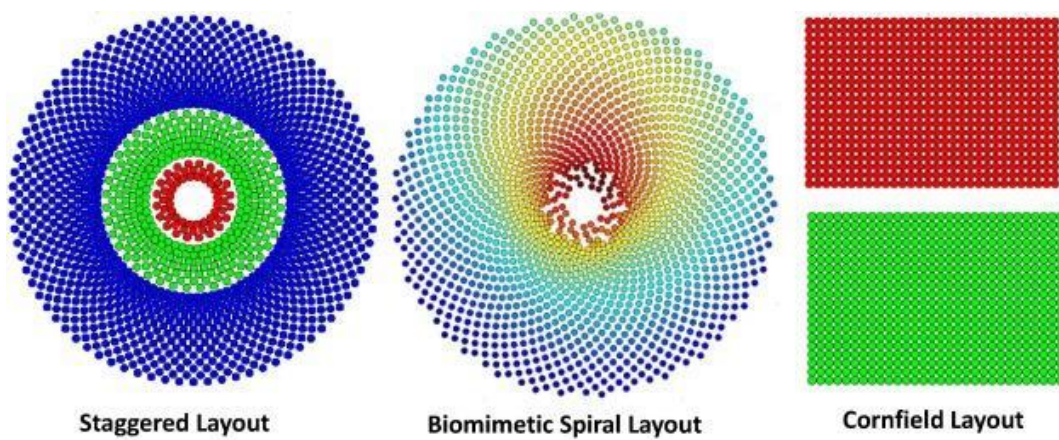


Figure 1. 5. Traditional CSP field layouts [15].

## 1.7 Heat Transfer Fluid (HTF)

A heat transfer fluid is used to absorb heat from the receiver and produce steam for power generation. In commercial solar power towers, three HTFs are used: molten salt, water/steam, and air. Usually in solar troughs, water acts as HTF, being heated to steam, turbines and generators are subjected to convert the energy in water to electrical energy. However, when it is about generating power consistently through day and nighttime, the concept of storing heat energy comes into the scenario. Molten salt in these cases is the most popular option.

### 1.7.1 Thermal Energy Storage (TES)

As we strive to harness the sun's power efficiently, the significance of thermal energy storage in Concentrated Solar Power (CSP) systems cannot be overstated. Innovations in this realm are key to overcoming the intermittent nature of sunlight. Various strategies are employed, each with its unique advantages and challenges. Other than molten salt, currently in Thermal Energy Storage systems-

- a. Alkali Nitrates are being used and among them  $\text{LiNO}_3$  is the one providing large temperature range. However high cost of this additive is a drawback for their development.
- b. Doping Nanoparticles ( $\text{SiO}_2$  and  $\text{Al}_2\text{O}_3$ ) with 1wt% of nanoparticles increases the heat capacity by 20% in some cases, also may enhance thermal conductivity.
- c. Using carbonate or chloride in the molten salt chemistry to achieve higher thermal to electric conversion.
- d. Nitrates are unstable at temperature higher than above  $600^\circ\text{C}$ . 60wt%  $\text{NaNO}_3$ , 40wt%  $\text{KNO}_3$  is being used nowadays [16]

## 1.8 Optical Efficiency ( $\eta_o$ )

The performance parameter at the forefront of this investigation is optical efficiency ( $\eta_o$ ) [17], a composite measure comprising several crucial factors. This efficiency value represents total efficiencies of the receiver and solar field. Central to this assessment is the

## Chapter 1

nuanced understanding of the cosine effect, encapsulated within cosine efficiency. As heliostats dynamically position themselves to reflect sunlight to the receiver tower, factors like the sun's position and individual heliostat placement influence this efficiency. Shadowing efficiency comes into play when one heliostat casts a shadow on another, diminishing the available solar radiation. Blocking efficiency enters the scene when a heliostat obstructs sunlight from reaching its neighboring counterpart. Completing the quartet, intercept efficiency accounts for losses when reflected sunlight fails to reach the receiver, capturing the nuances of spillage loss. The culmination of these efficiencies is encapsulated in the overarching optical efficiency, a pivotal parameter in heliostat layout studies within the realm of CSP systems.

- a. **Cosine efficiency:** Cosine effect is the most important efficiency parameter of a heliostat field. The amount of sunlight that can be captured by a surface is maximized when it is held perpendicular to the sun's rays. However, for SPT plant, heliostat is positioned so that it can reflect incident radiation to the receiver tower. By tracking mechanism, surface normal of the heliostat is so positioned that it bisects the angle between the sun's rays and a line connecting the heliostat to the tower. The effective reflection area of a heliostat is reduced by this effect known as cosine effect and efficiency regarding this effect is known as cosine efficiency. Cosine efficiency depends on the following two conditions [13]:
  - i. The sun's position in the sky. Therefore, it varies as the day and hour of the day changes.
  - ii. The position of an individual heliostat in the field. Hence, for different heliostat, cosine efficiency is also different.
- b. **Shadowing efficiency:** When a heliostat casts a shadow on another heliostat which is situated behind it thereby reducing the amount of solar radiation that can be fallen on it. This is known as shadowing.
- c. **Blocking efficiency:** Blocking occurs when a heliostat blocks the reflected sunlight from another heliostat located behind it. The amount of radiation reaching the receiver is reduced by this effect.

d. **Intercept efficiency:** Losses occur when reflected sunlight from the heliostat field fails to intercept or impinge on the receiver. Image intercept efficiency accounts for this loss which is also referred to as spillage loss. Light that falls on non-absorbing surfaces on the receiver such as refractory walls, pipes or the tower structure is accounted for in this efficiency.

Optical efficiency is the value that represents all the efficiencies and is found by the product of all four members. For heliostat layout related studies this parameter is the most prominent one [13]

### 1.9 SolarPILOT

To evaluate the optical efficiency, an open-source software SolarPILOT is used for the design, characterization, and optimization of the concentrated solar power plants. This tool has been introduced by Wagner and Wendelin [18] and they have provided information on the SolarPILOT code in detail in their study.

SolarPILOT utilizes its database on weather based on the location. Therefore, no extra care about solar angles or earth data is required. Date and time data can be set manually to simulate the layout performances for the intended location. In the case of layouts SolarPILOT has radial staggered and corn field layouts built. Other than these layouts can be imported manually. Layout data consists of heliostat coordinates, irradiation aim point at receiver in three directions. All the data for a layout can be generated and imported manually in this software. In terms of results, this software provides a various range of efficiency parameters such as blocking efficiency, shadowing efficiency, attenuation efficiency, image intercept efficiency, cosine efficiency, power incident on the field, power absorbed by the HTF, Power absorbed by the receiver, cloudiness efficiency, absorption efficiency, reflection efficiency, incident flux. SolarPILOT also generates a cost for the plant data, however in case of user input layout this cost estimation may vary depending on the geographic, geometric orientation of the layout and location.

### **1.10 Scope of the Thesis**

The radially staggered layout used by the presently available CSPs cannot be installed in hilly areas since the layouts are designed for flat surfaces and may result in a conical shaped layout with less optical efficiency. Therefore, to utilize the whole potential of the hilly areas, a thorough investigation is conducted on the proposed inclined layout and the resulted optical efficiency will be compared with the efficiency of Crescent Dunes, Tonopah, to compare how well the present HCSP system performs.

Chapter 2 delves into the crucial aspect of field layout design for solar thermal powerplants, emphasizing its impact on optical performance. Traditional radial staggered methods have dominated, however new layouts like biomimetic spirals are gaining traction. Hillside installations are explored for their potential cost advantages but face challenges in heliostat installation on steep terrain. Additionally, the use of molten salts for energy storage and various software programs highlights the diverse technological aspects covered in this comprehensive literature review.

Chapter 3 navigates the intricate terrain of 3D field layout design for solar thermal powerplants, focusing on an inclined surface layout. The chapter introduces a novel approach, using real coordinates from Google Earth, and explores three different geographical locations with varying DNI. The chapter provides a comprehensive exploration of physical modeling for optimal solar field layouts.

Chapter 4 explains the mathematical intricacies in solar thermal powerplant modeling using SolarPILOT. It covers the Hermite analytical method for solar flux simulation, incorporating Hermite polynomials. Techniques for shadowing and blocking efficiency involve vector projection and clipping methods. Cosine efficiency is calculated by considering the ratio of incident power on the heliostat field. The image intercept factor, a computationally expensive aspect, is addressed with a hybrid approach using a zonal approximation. Overall, the chapter provides a concise overview of the mathematical models applied in SolarPILOT for efficient solar thermal powerplant design.

## Chapter 1

Chapter 5 validates the solar thermal powerplant model by reproducing studies conducted by Wagner and Wendelin and Ashikuzzaman and Adnan. The comparison with Wagner and Wendelin's simulation using 8731 heliostats, reveals close alignment in key parameters. Furthermore, the layout and optical efficiency of Crescent Dunes CSP, as studied by Ashikuzzaman and Adnan, are regenerated and simulated using a C program and SolarPILOT, respectively.

Chapter 6 is the results and discussions of the study, particularly focusing on the potential of an inclined V-shape layout in hilly areas for three different locations in the USA. The investigation evaluates the layout's performance in terms of blocking efficiency and receiver flux profile at different times and dates throughout the year. The study concludes with an optical efficiency analysis, comparing the three locations, and an evaluation of two potential sites based on individual efficiency parameters. The chapter concludes by highlighting the overall potential of the sites for a Hillside Concentrated Solar Power (H-CSP) project, emphasizing the need for further economic considerations like Levelized Cost of Electricity (LCOE).

The study concludes by investigating the optical efficiency of an inclined V-shape layout designed to harness solar energy in rocky or non-green hill areas across three different locations in the United States. Practical considerations led to the selection of two optimal layouts from various test configurations. Despite Site 2 exhibiting slightly lower optical efficiency than Site 1, it emerges as a compelling candidate for hosting a Hillside Concentrated Solar Power (H-CSP) plant.

### Literature Review

#### 2.1 Field layout

Field layout design stands out as a critical consideration in various studies, holding significant sway over the optical performance of the field. Notably, a substantial portion of the overall investment is allocated to the heliostat field expenditure [19]. Traditionally, many commercial plants have embraced the radial staggered method, a concept introduced by Lipps et al. in the 1970s [20].

In a comparative analysis by Gadalla et al., two newly proposed layouts, Campo radial-staggered and biomimetic spiral layouts, were examined [21], Figure 2.1 visualize these two layouts. The layouts underwent optimization considering different objectives, including thermal and economic constraints on design variables like tower height, receiver dimensions, and heliostat dimensions.

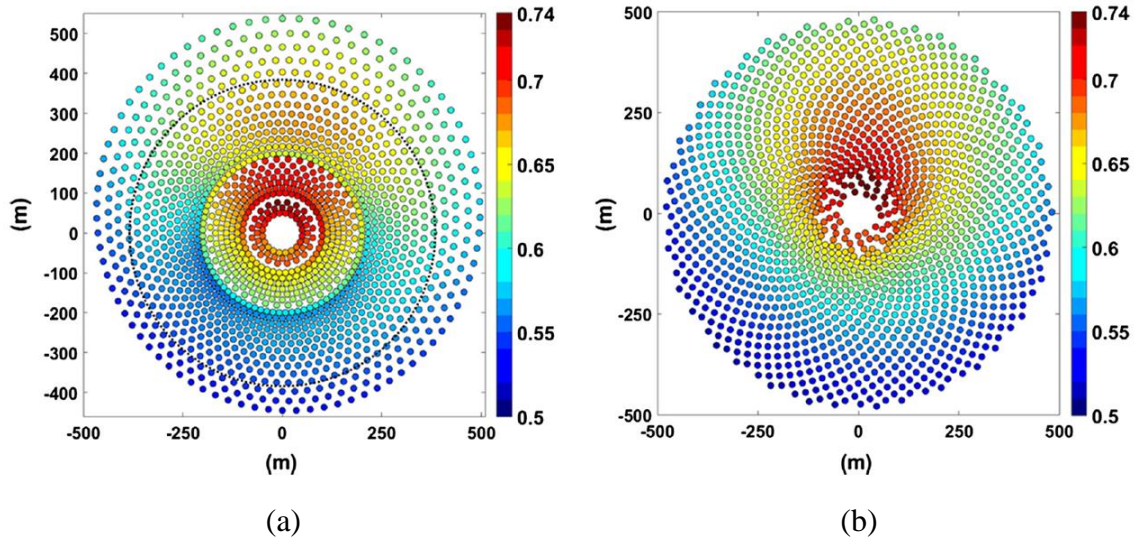
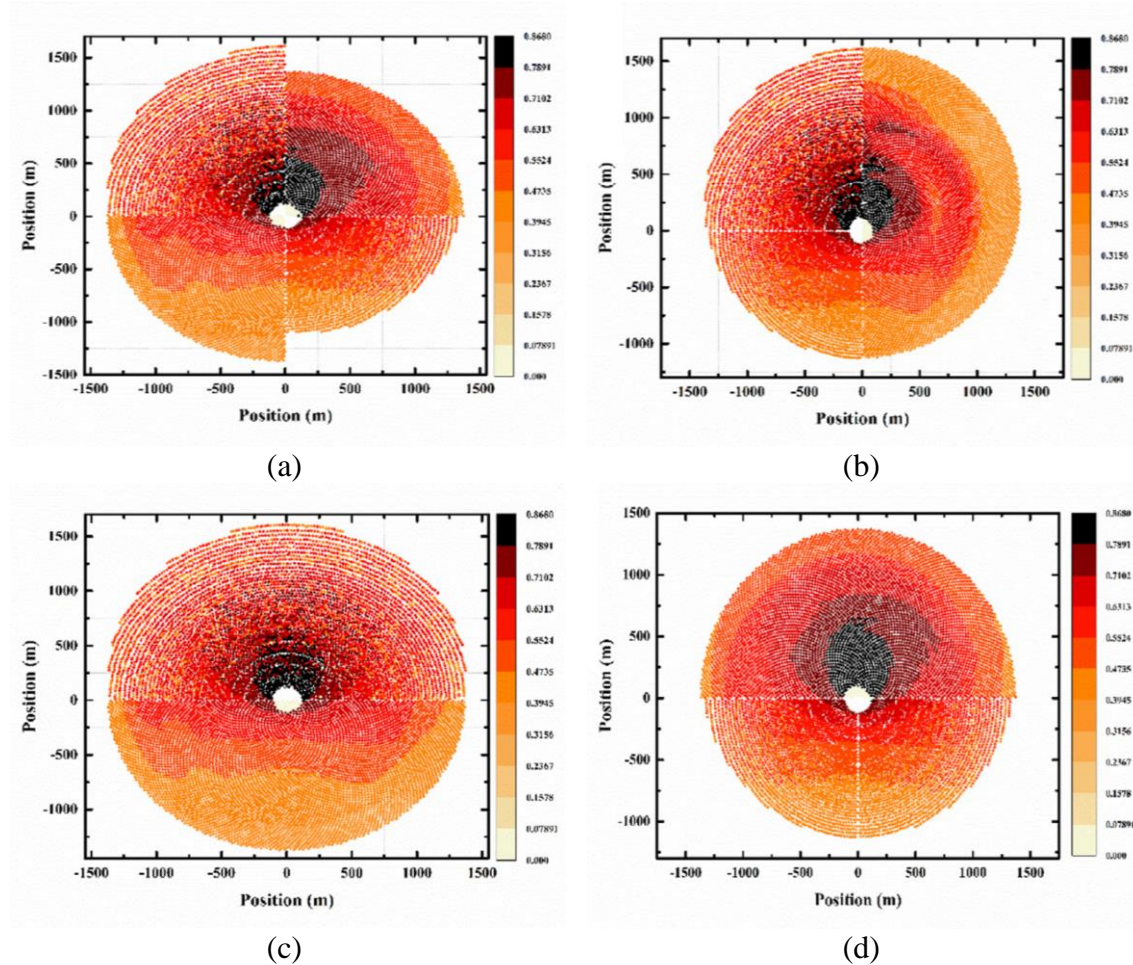
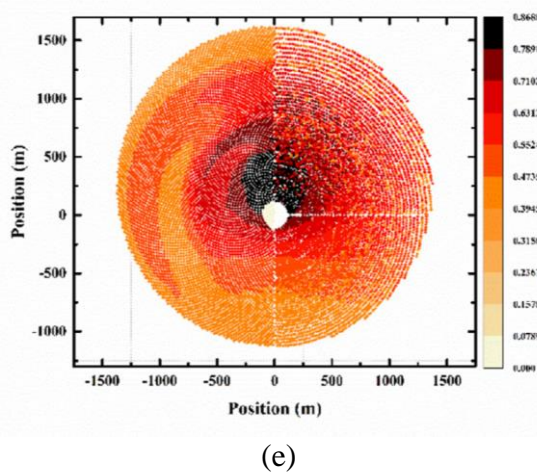


Figure 2. 1. Optimized field layout with weighted efficiency as the objective (color scale represents the annual weighted efficiency for every heliostat within the field), (a) Campo radial-staggered, (b) biomimetic spiral [21].

## Chapter 2

Examining circular fields, Zhang et al.[22] explored two layouts—radial staggered and biomimetic spiral—revealing that the staggered layout outperformed the biomimetic one in terms of optical efficiency. Despite this, it had smaller area requirements. The study also delved into the variation of optical efficiency concerning plant capacity, proposing, and testing several combinations of both layouts. Some combination layouts demonstrated superior performance compared to the original two kinds of layouts [22]. A similar study for the surrounding field, favored the biomimetic spiral over the radial staggered field [23]. Recently, a lot of interest has been shown in the biomimetic spiral layout by Noone et al. [5]. The performance of several distinct hybrid configurations is studied by Ashikuzzaman and Adnan [24] pictured in Figure 2.4 and after doing a thorough investigation into layout design, a novel layout called Fractal was introduced.





(e)

Figure 2. 2. Optical efficiency of (a) hybrid 1, (b) hybrid 2, (c) hybrid 3, (d) hybrid 4 and (e) hybrid 5 on the summer solstice generated by Ashikuzzaman and Adnan.

Hybrid layout 1 features a staggered arrangement radiating outwards in the northwest and southeast sections. When the staggered heliostats in the eastern portion are substituted with a biomimetic design, Hybrid-2 (H2) is formed, leaving only the western side staggered. Hybrid-3 (H3) results from retaining the staggered layout solely in the northern part, while adopting a biomimetic layout in the southern region. Conversely, Hybrid-4 (H4) emerges when the staggered heliostats in the north are replaced with a biomimetic pattern, leaving only the southern side staggered, thus presenting the opposite of H3. Lastly, Hybrid-5 (H5) is created by replacing heliostats positioned in the west with a biomimetic layout in the western part and a staggered pattern in the east.

## 2.2 Heat Transfer Fluid

Characteristics required for HTF include low melting point, high boiling point, low corrosion and viscosity, high thermal conductivity, high heat capacity for storing energy and low cost [25][26]. For plants with storage system molten salt is used to store thermal energy as well as to produce steam. Molten salts are the most commonly used HTF in solar power tower plant due to their High heat capacity, Low viscosity and corrosive property and high working temperature ( $> 500^{\circ}\text{C}$ ) [10]. Molten salts typically consist of 60% sodium nitrate and 40% potassium nitrate [27].

### **2.3 Simulation software**

UHC, DELSOL3, HFLCAL [28], TieSOL [29] can be utilized for generating solar field geometry by code. Other programs are capable of calculating detailed field characterization but lacks the capability to generate and optimize optical problems quickly. For example, MIRVAL [30], it is a Monte Carlo program which calculates the heliostats (mainly 4 types) and a segment of receiver (mainly 3 types) interaction. Another program is STRAL [31], the main purpose is to calculate the flux density of the heliostat field layout with a very high accuracy within a relatively small amount of calculation time. Moreover, to calculate annual performance of tower systems, System Advisory Model (SAM) [32] is an effective program along with TRNSYS [33]. Finally, SolarPILOT; the open-source software introduced by Wagner and Wendelin, is found to be the most convenient one to perform the simulation-based tasks related to this study.

### **2.4 Motivation of the present investigation**

Recent investigations were conducted for horizontal fields of heliostats where the first and the last layer of heliostats are at an average distance of one or more kilometers. It eventually increases the distance between the solar tower and the outer heliostats. On the other hand, it can be mathematically shown that a hillside inclined plane reduces this distance between the receiver and the nearest layer and furthest layer of heliostats. Also, in comparison to conventional CSP sites, hillside heliostat fields have lower capital costs because they do not need flat ground. However, heliostat installation on steep terrain could be a drawback of hillside installations [34]. Afterwards, Noone et al. [35] introduced a tool considering cosine, shadowing, and blocking efficiency to locate the sites for central receiver of solar thermal powerplants in hillside terrain. Therefore, delve into the potential of hillside terrains as a CSP site is the key intention of this study considering optical efficiency as a key parameter.

## Physical Modeling

### 3.1 V-shape inclined plane

The layout of the present study and the existing one is plotted as shown in Figure 1(a) – (b). The central receiver is assumed to be within a small distance from the center of a sphere, the lower hemisphere generates the maximum closest points to the receiver as shown in Figure 1(a). Since the layout is in 3D, an evaluation of Z-axis has to be done along with the X and Y axis. Taking the East in the positive X direction facilitates the sun direction to fall near to the central axis of the layout. North is in the positive Y direction and variation in Z direction is also in the Y direction, with a relation-

$$Z = \begin{cases} Y, & \text{if } Y < 0 \\ Y, & \text{if } Y > 0 \end{cases} \quad (3.1)$$

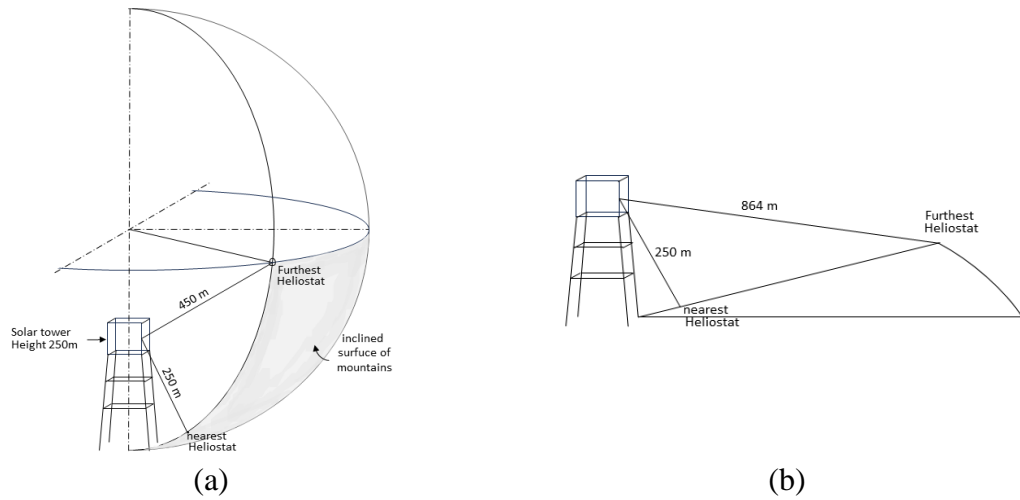


Figure 3. 1. Configuration of (a) the proposed inclined surface layout, and (b) the flat surface layout.

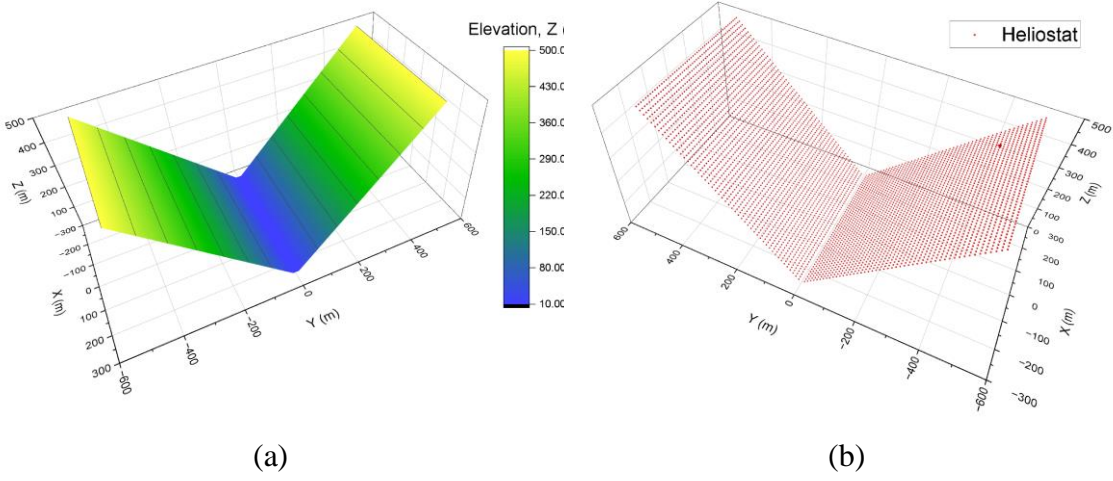


Figure 3. 2. Simplified generation of HCSP (a) V-shape layout for inclined hill surfaces, and (b) the array of heliostats (dots represent the heliostats in the field).

### 3.1.1 Locations and field parameters

This study is performed for three different locations, as mentioned in Table 1. A quantity of 5100 heliostats having an individual size of  $5\text{m} \times 8\text{m}$  are arranged as shown in Figure 2(a) - (b). The locations are chosen because of their geographical position which helps these hilly areas to generate more blocking efficiency and cosine efficiency in the morning and afternoon times. The diameter of the receiver is 17.65m and height is 21.6m with the overall tower height of 195m. The thermal absorptance of receiver is taken to be 0.94. Since, this layout produces a V-shape in three dimensions, regions near the tropic of cancer (declination angle,  $\delta$  or latitude =  $23.5^\circ$ ) are considered to have the least blocking. The selected locations receive Direct Normal Irradiation (DNI) of 4 to 7  $\text{KWh/m}^2$  per day according to the Solar Resource Map of USA shown in Figure 3.

## Chapter 3

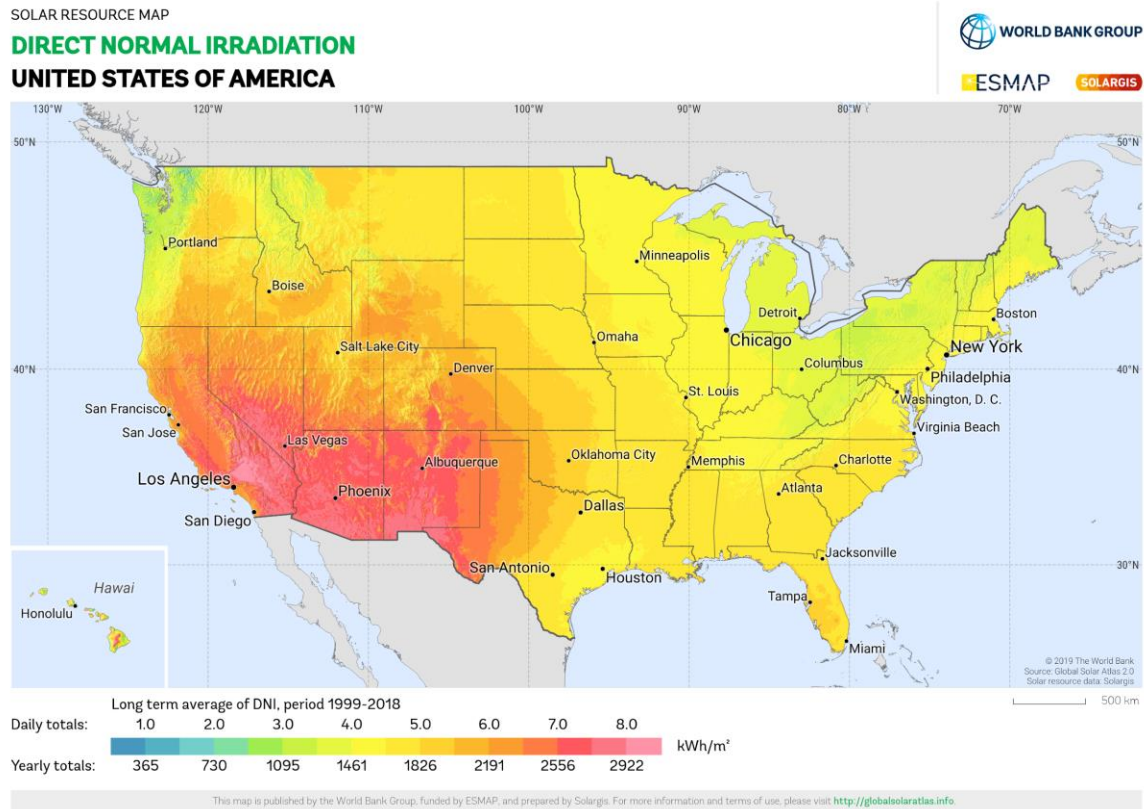


Figure 3. 3. Direct Normal Irradiation Map of USA [36].

Table 3. 1. Proposed field data and the location parameters from the SolarPILOT Database.

Location	Field Dimension	City	State	Latitude	Longitude	DNI	Elevation
Location 1	$X = 500\text{m}$	Blue					
		Canyon	CA	39.3°N	-120.717	5kWh/m <sup>2</sup>	1609
		Ap					
Location 2	$Y = 1000\text{m}$	Deer					
		Valley	AZ	33.68°N	-112.083	7kWh/m <sup>2</sup>	450
Location 3	$Z = 0 \text{ to } 500\text{m}$	Phoenix					
		Lufkin	TX	31.23°N	-94.75	8.5kWh/m <sup>2</sup>	96

Among these locations, Location 3 receives the most DNI, however latitude being the lowest than other two, overall power generation of a CSP throughout the year may not be matching the expected values. In a similar manner, Location 2 having latitude of 33.68° is not expected to produce much power throughout the year than the Location 1. Therefore,

## Chapter 3

Location 1 is the most appropriate one to locate sites for CSP plants, which is verified by the results discussed in Chapter 6 section 7. Potential site searching hence begins here.

### 3.2 Real hill surfaces

In the process of potential site searching, the primary task is to extract real coordinates for the solar receiver tower, which is completed using Google Earth. The elevation, width and length of the suitable solar field is then selected from Google Earth as well. Figure 3.4(a) - (b) shows the potential site locations on google earth.

#### 3.2.1 Field data and parameters

Heliostat dimensions are promoted to the one of the existing technologies that is  $12.2\text{m} \times 12.2\text{m}$ . The properties of the central receiver tower are kept constant such as: diameter and height of the receiver is 17.65m and 21.6m respectively with the overall tower height of 195m. The thermal absorptance of receiver is taken same as the previous simulations as well which has the value of 0.94. Table 2 shows the field data proposed for two sites in Location 1 (Location 1 is selected over the other two locations, based on the superior overall performance of the plant with the V-shape layouts).

Table 3. 2. Proposed field data for two sites in Location 1.

Data	Site 1	Site 2
Central Tower	39°12'09''N 120°36'46''W	39°01'20''N 120°30'53''W
Altitude	812.662m	1268.747m
South peak	39°11'01''N 120°36'46''W	39°00'46''N 120°30'09''W
Altitude	1588.4439m	1620.072m
Spread	2087.63m	1488.12m
Inclination	21.82°	13.655°
North peak	39°13'03''N 120°37'00''W	39°01'36''N 120°31'52''W
Altitude	1726.8255m	1599.402m
Spread	1682.35m	1515.19m
Inclination	30.24°	12.605°

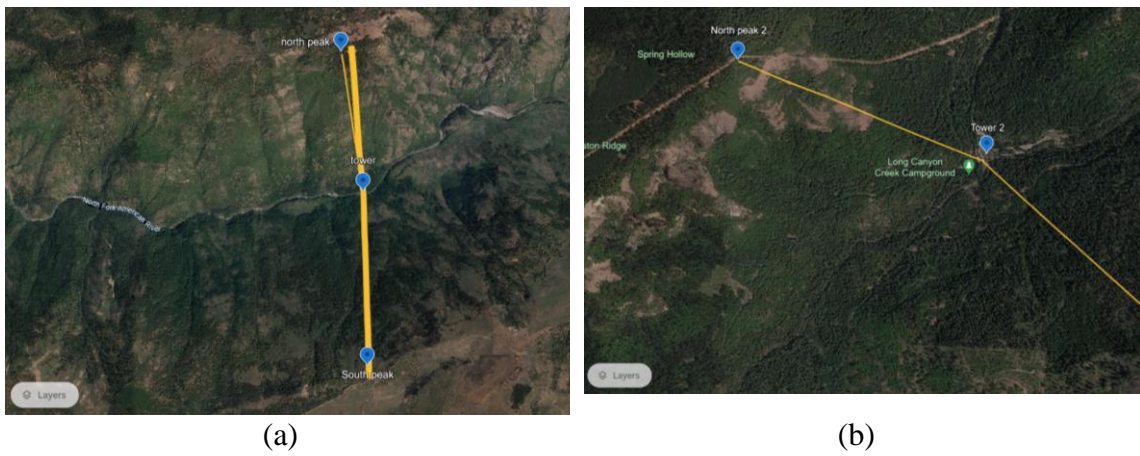


Figure 3.4. Suitable sites with north and south wing spread for (a) site 1 and (b) site 2.

### 3.2.2 Modelling real inclined surfaces

To model the real inclined surfaces, a handsome number of coordinates has been selected and some common formulas has been applied to iterate the points residing within them-

$$\tan \theta = \frac{y}{x}; \quad \{0^\circ < \theta < 180^\circ \quad -0^\circ < \theta < -180^\circ\} \quad (3.2)$$

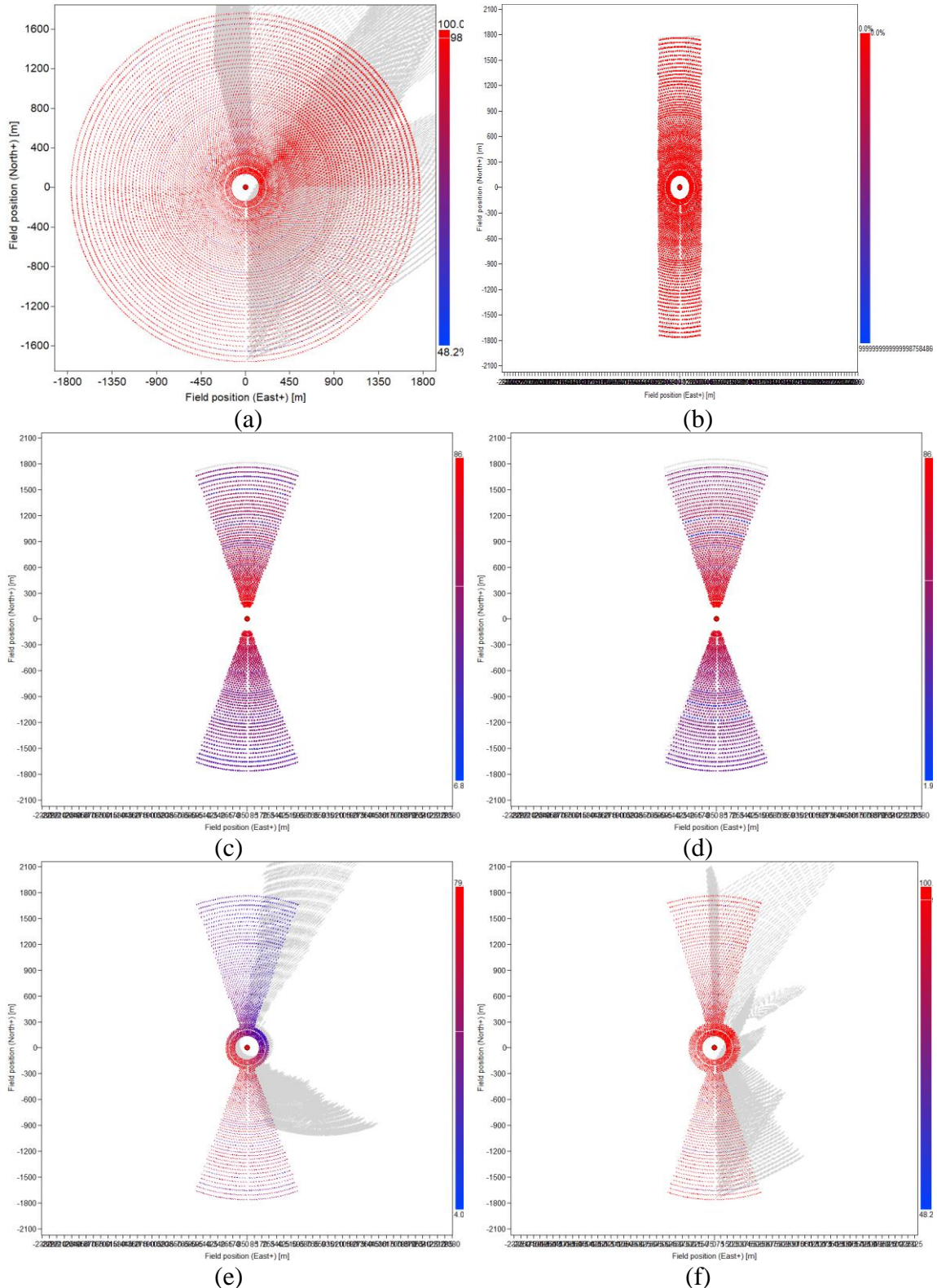
$$z = |x| \cdot \sin \sin \phi \quad (3.3)$$

$\theta$  is the radial angle and  $r$  being the normal direction of a point from the center or the receiver tower;  $x$  and  $y$  are the cartesian coordinates for the heliostats and  $\phi$  is defined as the inclination angle. 26 test-layouts has been tested on the selected sites and two are found to be working efficiently.

### 3.2.3 Optimum layout for Site 1

The shape of the layouts projects radial staggered pattern having two opposing Pie shapes, with heliostats stacked in full circles near the receiver tower for several layers, on a 2D plane. Radial staggered pattern is chosen over the simple V-shape array pattern or other patterns like cornfield or Biomimetic spiral, because of it's supreme performance over others on the horizontal CSP layouts. It is expected that, implementing radial staggered pattern on to the inclined surfaces would result in better efficiency. Figure 3.5(a)-(g) depicts some of the tested layouts for site 1.

## Chapter 3



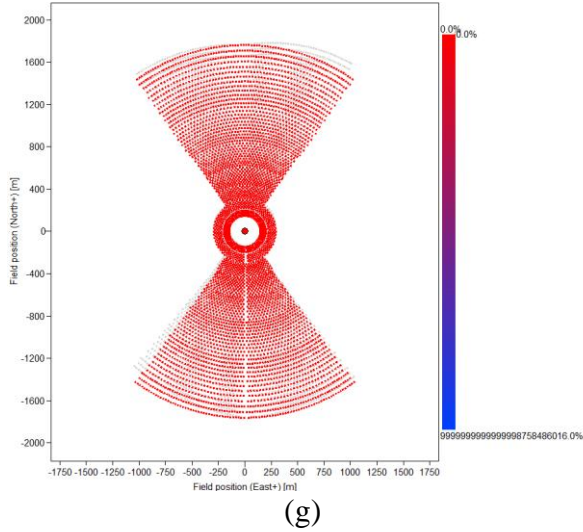


Figure 3.5. Test Layouts for Site 1 (a) Test Layout 1, (b) Test Layout 2, (c) Test Layout 3, (d) Test Layout 4, (e) Test Layout 5, (f) Test Layout 6, (g) Test Layout 7 to find out the optimum layout for Site 1.

Table 3.3. Test Layout properties for Site 1.

<b>Test Layout</b>	<b>Heliostat Count</b>	<b>Efficiency (%)</b>
1	11206	63.03
2	3216	Impractical
3	2430	59.95
4	2430	63.34
5	2765	65.9
6	2736	71.8
7	4850	Impractical

In Figure 3.5(a) – (g) some of the test layouts for site 1 are shown and their properties are displayed in TABLE 3.3 where all the efficiencies are measured under standard conditions and on June 21<sup>st</sup> at 3.00 pm.

Test Layout 1 is direct projection of radial staggered pattern on the real surface of site 1. Resulting in an optical efficiency of 63.03%. The reason behind this is the taco bell shape of the layout; during the morning and afternoon when sun is laying on a side this layout generates huge blocking and shadowing effects. This adverse effect might be visible in case to winter months too.

Test Layout 2 is based on the inclined V-shape layout with the difference of one having heliostats organized in a simple array type arrangement and the later one is projection of the radial staggered pattern. In the surface of site 1 this layout produces impractical values of efficiency due to the geometrical nature of the site.

## Chapter 3

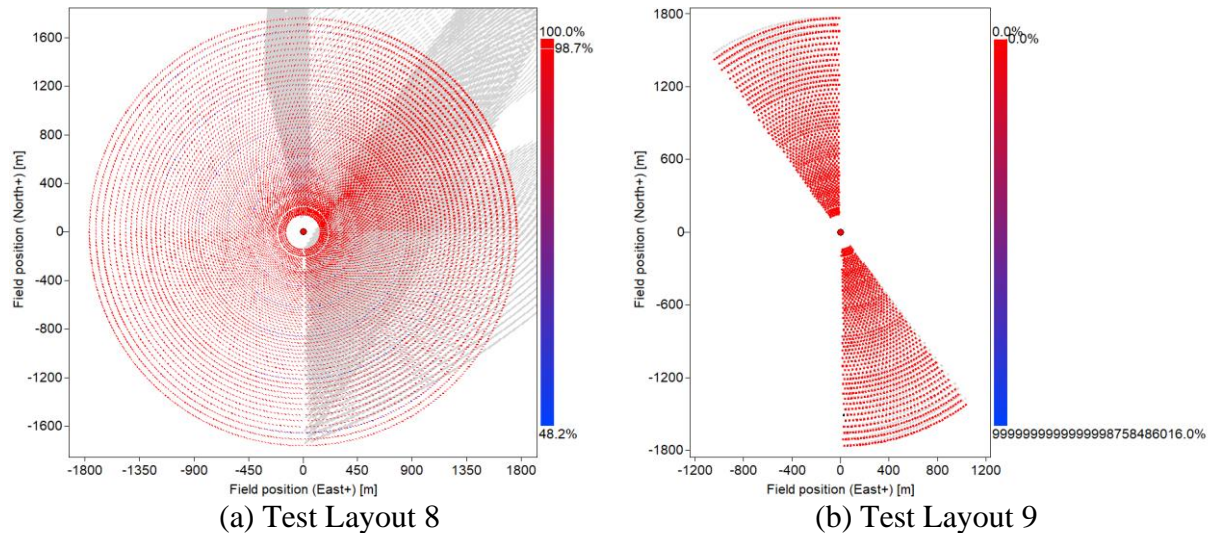
From Test Layout 3 to 6, it is observed that condensing heliostats near to the receiver tower gradually increases efficiency. However, from the further study, decrement rather than increment is observed in efficiency. In these layouts the angular spread is taken around  $36^\circ$  on each wing from the central receiver tower.

Test Layout 7 is a depiction of the result of change in the angular spread. Due to the nature of the geometrical surface increment in angular spread becomes impractical, due to a large portion of heliostats experiencing huge blocking factor. Decrement in angular spread decreases efficiency expectedly.

Hence, Test Layout 6 has been found to be the most optimum one for Site 1.

### 3.2.4 Optimum layout for Site 2

A similar approach as for site 1 is also taken to determine the optimum layout for site 2. Figure 3.6(a) – (f) shows some of the tested layouts for site 2 and Table 3.4 displays the properties of those layouts.



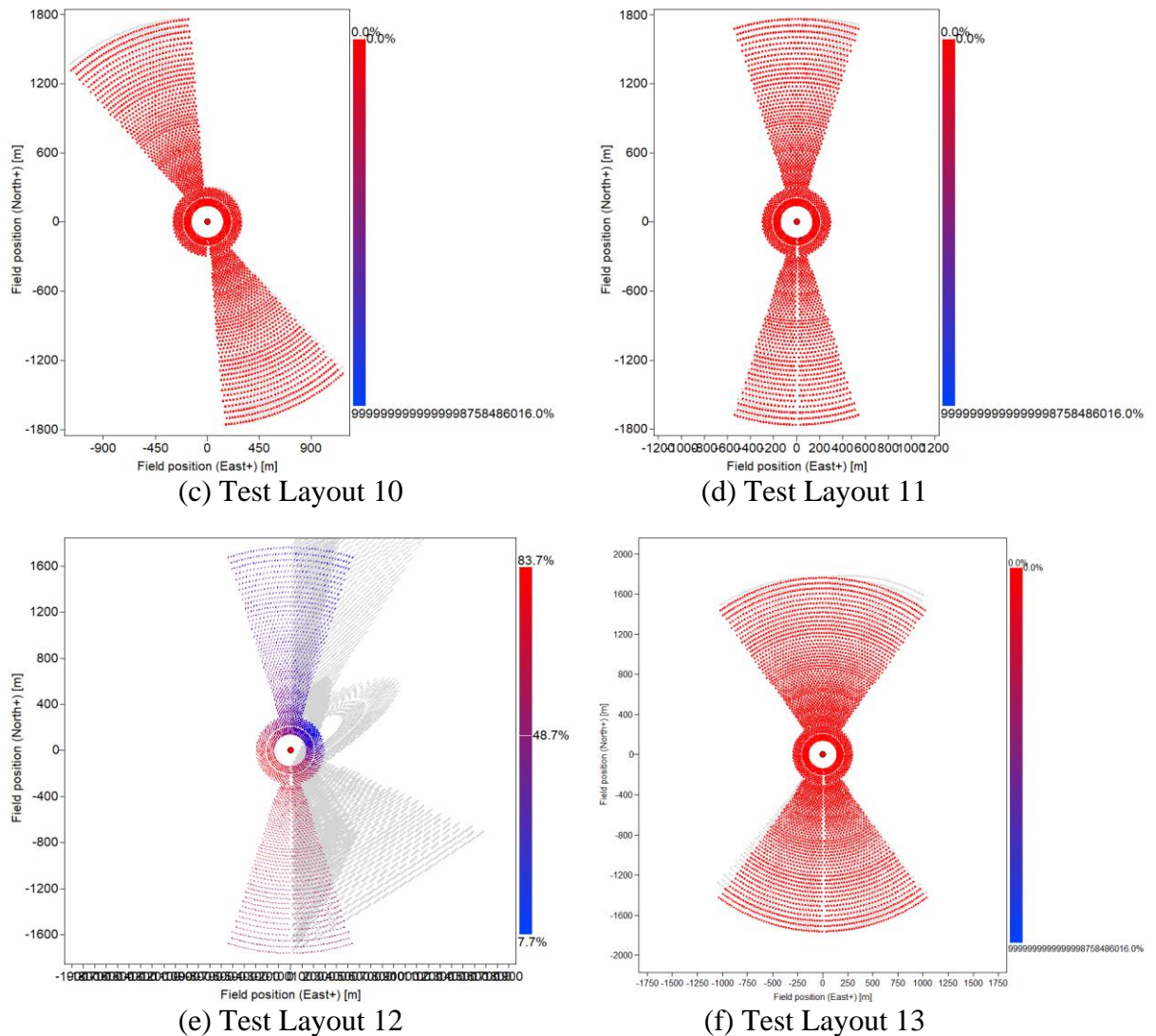


Figure 3. 6. Test Layouts for Site 2 (a) Test Layout 1, (b) Test Layout 2, (c) Test Layout 3, (d) Test Layout 4, (e) Test Layout 5, (f) Test Layout 6, to find out the optimum layout for Site 2.

Site 2 is a bit centered to the South-East axis, although Test Layout 9 here in site 2 is also direct projection of radial staggered pattern on to the inclined surfaces. Results in efficiency of 61.47%. The reason is similar to the test layout 1 in site 1.

Test Layout 9 and 10 properly enables to visualize the appropriate intended layout on site 2. However, due to some ridge like area within the layout these two test layouts provide impractical values for efficiency, whereas Test Layout 11 provides impractical values due

## Chapter 3

to much dense heliostats near to the central receiver tower. This increases the blocking and shadowing factor.

Table 3. 4. Test Layout properties for Site 2.

<b>Test Layout</b>	<b>Heliostat Count</b>	<b>Efficiency (%)</b>
8	11182	61.47
9	2217	Impractical
10	2831	Impractical
11	2736	Impractical
12	2736	71.5
13	4795	Impractical

Test Layout 12, however, with 11 full circular layers of heliostats near to the central receiver tower resulting in 71.5% of efficiency. Densing more heliostats is obstructed by some ridges on the site, that increases the blocking factor immensely.

A similar impractical behavior such as Test Layout 7 is exerted by Test Layout 13 due to expansion of the angular spread of the layout. Therefore, for site 2, Test Layout 12 is to be considered in further study undoubtedly.

### Mathematical Modeling

#### 4.1 Solar flux simulation

Wazel et al. [37] found it practical to establish an image plane as shown in Figure 4.1, positioned at the receiver's center, perpendicular to the line connecting the receiver's center to the representative heliostat's center, known as the optic axis. The intensity of reflected sunlight on this image plane from a single representative heliostat is denoted as  $F(x, y)$ .  $F$  can be effectively expressed as the convolution of  $M$  and  $S$ .

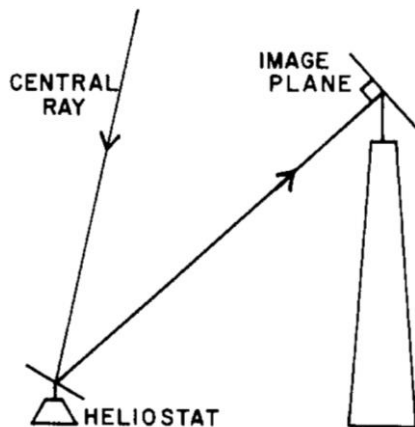


Figure 4. 1. Relation between heliostat, the sun, and the position of the image plane [37].

$M$  signifies the brightness distribution on the image plane that a heliostat would produce if the Sun were a point source. In the case of a perfectly flat reflector,  $M$  is derived by projecting the luminous area of the mirror onto the image plane.  $S$  represents the normalized flux density distribution on the image plane caused by an infinitesimal element on the heliostat surface, resembling a pinhole image of the limb-darkened solar disc. Lastly,  $F$  undergoes convolution with a third function,  $G$ , portraying the statistical distribution of errors in the reflection angle. This convolution yields  $F$ , illustrating the flux density distribution on the image plane due to a population of heliostats within a specific cell of

## Chapter 4

the collector field model at a given time during the day. Analytically equation for  $F(x, y)$  is as follows-

$$F(x, y) = M(x, y) \cdot S(x, y) \cdot G(x, y) \quad (4.1)$$

SolarPILOT utilizes Hermite analytical method for solar flux simulation. This is a more refined approach to explain the error shape in two dimensions [37]. The analytical form of the flux intensity profile can be given as-

$$F(x, y) = \frac{1}{2\alpha_x \alpha_y} \exp \left[ -\frac{1}{2} \left( \frac{x}{\alpha_x} \right)^2 - \frac{1}{2} \left( \frac{y}{\alpha_y} \right)^2 \right] \cdot \left\{ \sum_{i=0}^{\infty} \sum_{j=0}^{i} A_{i,j} H_i \left( \frac{x}{\alpha_x} \right) H_j \left( \frac{y}{\alpha_y} \right) \frac{1}{i! j!} \right\} \quad (4.2)$$

where,  $H_i$ ,  $H_j$ ,  $A_{i,j}$  are the Hermite polynomials used to modify the intensity at any position  $(x, y)$ . An example of Hermite polynomials is as follows and  $n$  being a real constant-

$$H_n(x) = \sum_{r=0}^m (-1)^r \cdot \frac{n!}{r!(n-2r)!} \cdot (2x)^{n-2r};$$

$$\text{where, } m = \begin{cases} \frac{n}{2}, & \text{when } n \text{ is even} \\ \frac{n-1}{2}, & \text{when } n \text{ is odd} \end{cases} \quad (4.3)$$

The components of the coefficients are evaluated for a given sun shape, mirror geometry, optical error contributions, and relative position to the tower. Two coefficients  $\alpha_x$ ,  $\alpha_y$  represent the standard deviation of the image distribution in  $x$  and  $y$  direction relative to the image plane.

### 4.2 Shadowing efficiency

SolarPILOT calculates shadowing and blocking using vector projection and clipping method. Neighboring heliostats are tested for potential interference by projecting vectors from the heliostat corners along the direction of either the tower (blocking) or sun position (shadowing). If a projected vector intercepts an adjacent heliostat, blocking or shadowing are enforced according to the position of the interception.

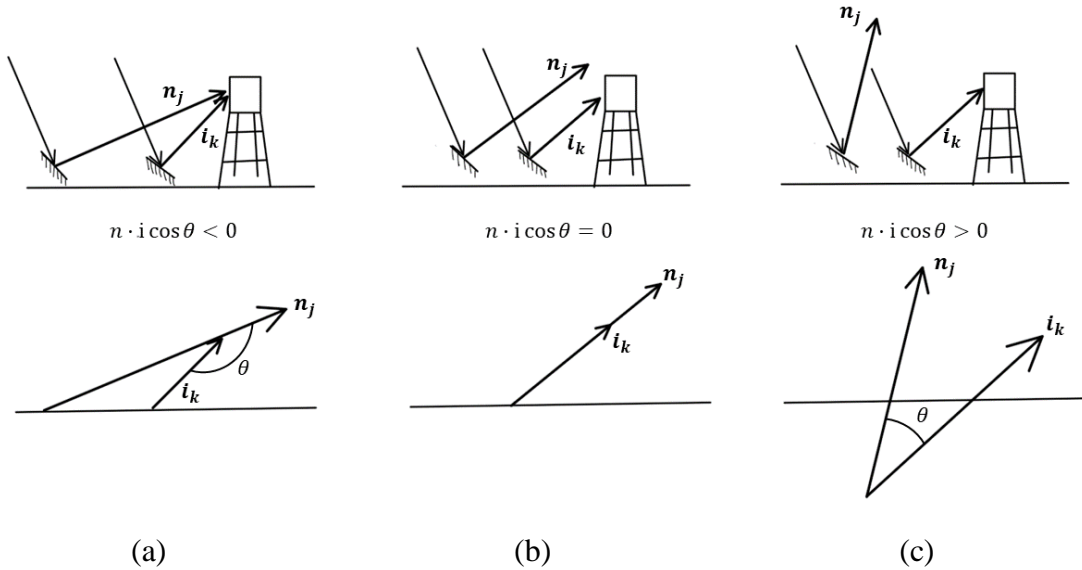


Figure 4.2. Heliostat normal vector and interfering heliostat subject vector orientations  
 (a) depicting zero loss, (b) having dot product value of zero and (c) with positive dot product.

This method assumes that neighboring heliostats lie in parallel planes, which holds for all however very small solar fields in which tracking angles differ significantly between neighboring heliostats. This ji assumption results in the simplification that shadowed or blocked regions are rectangular, which simplifies the computation without affecting accuracy. Each heliostat J is assigned a list of neighbors that may block or shadow (“interfere” with) the heliostat. An interfering heliostat is subsequently denoted K. Heliostats are tested for the possibility of interference: a. The first test requires that the interfering heliostat K is within view of the interfered heliostat J. The dot product is calculated between the heliostat normal vector and the interfering heliostat subject vector.

$$v = \hat{n}_J \cdot \hat{i}_k \quad (4.4)$$

If the dot product is non-positive, K cannot interfere with J and the loss is zero.

### 4.3 Cosine efficiency

SolarPILOT calculates cosine efficiency is calculated in the same manner by taking the ratio of power incident on the aperture area of the heliostat field divided by the available power after cloudiness and shadowing losses. Cosine loss is evaluated for each heliostat by taking the dot product of the heliostat normal vector and the sun vector.

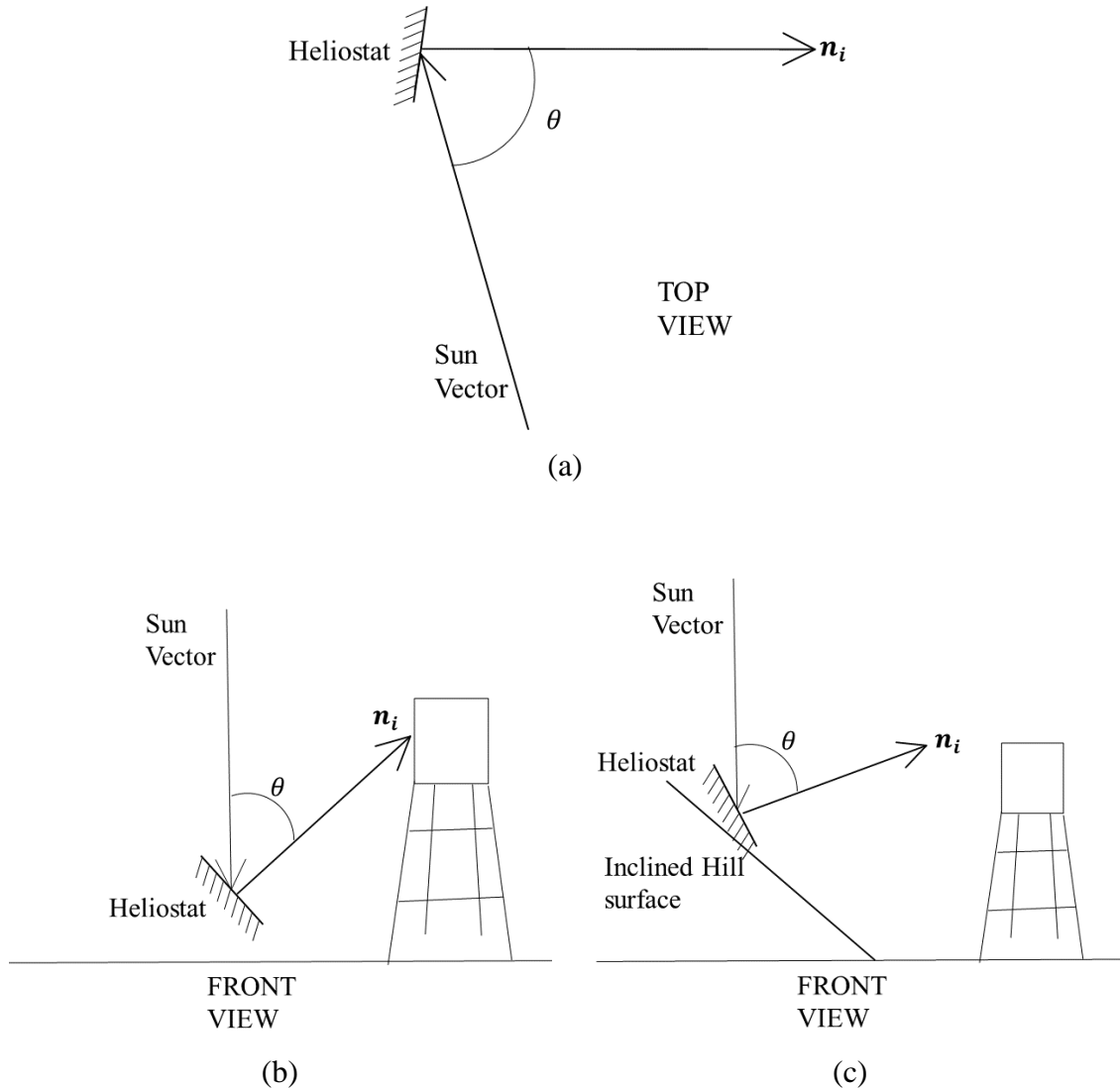


Figure 4. 3. Sun vector and Normal vector orientation in the morning (a) and at noon in (b) flat horizontal layouts and (c) H-CSP layout.

#### 4.4 Image intercept factor

Optical intercept factor (the amount of light captured by the receiver from any heliostat image) is equally significant but is comparatively much more expensive to calculate. SolarPILOT implements a novel method for dynamic heliostat grouping to reduce the expense of intercept factor evaluation, methods for approximating annual productivity with a subset of time steps throughout the year. SolarPILOT thus adopts a hybrid approach of calculating simple losses such as cosine and attenuation individually and the expensive

## Chapter 4

intercept factor loss using a zonal approximation at resolutions sufficient to maintain accuracy. The challenge with the zonal approach is that the intercept factor can depend strongly on position and change in intercept factor is nonlinear as a function of radial and circumferential position. SolarPILOT subdivides the heliostats, accordingly, creating a mesh in circumferential coordinates which has varying density in both azimuthal and radial dimensions.

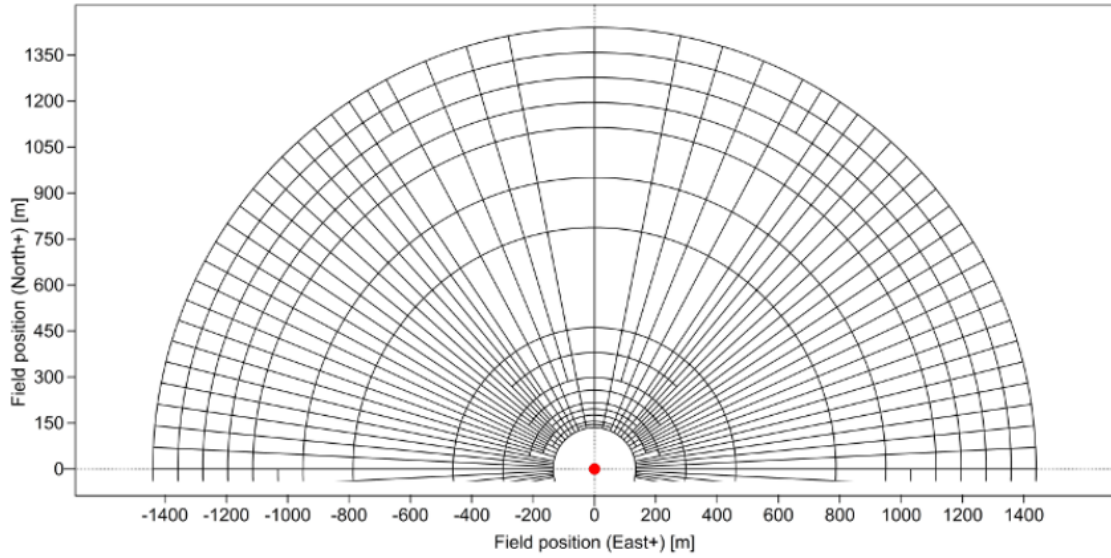


Figure 4. 4. A typical subdivision generated by SolarPILOT in a typical circumferential coordinate having varying density in both radial and azimuthal dimensions [18].

The zone to which a heliostat should belong is computationally nontrivial to determine. In the worst case, the number of assignment computations would be equal to the product of the number of zones and the number of heliostats. To circumvent this problem, we have devised a binary element tree extending readily available examples that guarantees that a small number of computations  $n_{cmax}$  are required to locate a heliostat within some tolerance  $\delta$ .

$$n_{cmax} \leq 2 \left[ \log \log (2)^{-1} \cdot \left\{ \log \log \left( \frac{\Delta r}{\delta r} \right), \log \log \left( \frac{\Delta \beta}{\delta \beta} \right) \right\} \right] \quad (4.5)$$

The binary element tree that groups heliostats together for intercept factor calculation divides the coordinate space into halves – radially and azimuthally. Each half is then

## Chapter 4

divided again and again until the size of the zone is sufficiently small. Divisions are done alternately between radial and azimuthal directions.

### 4.5 Single simulation point

The field performance is evaluated at a single sun position and solar resource. Each heliostat's performance is described by a single production value.

### 4.6 Extraterrestrial radiation

Weather file data is used as Insolation model. This model makes use of the extraterrestrial solar radiation, and this quantity varies by location and throughout the year and is calculated by-

$$\delta_0 = 1.353 + 0.045 \cos \cos \left( \frac{2\pi(u+10)}{365} \right) \quad (4.6)$$

Here,  $\delta_0$  is the Extraterrestrial radiation intensity ( $\text{kW/m}^2$ ) and  $u$  is the Day number of the year. DELSOL3 clear day is used as the atmospheric attenuation model in the SolarPILOT to get the regional atmospheric conditions.

## Chapter 5

### Model Validation

#### 5.1 Study of Wagner and Wendelin

In the study of Wagner and Wendelin [18], the tool SolarPILOT has been introduced as an extension of DELSOL3 and a data set is simulated for 20<sup>th</sup> March at 12:00. Mimicking those data set, a simulation has been performed in the current study for 8731 heliostats having a dimension of 12m × 11.83m. The height of the solar tower is 203.3m and receiver height and diameter are 20.41m and 17.67m respectively. The receiver had an absorptance of 0.94 with a radial staggered layout. Thermal power output and reference DNI are about 669.9 MW, 950W/m<sup>2</sup> respectively. The maximum field radius is 9 times the tower height and azimuthal spacing factor is 1.96. The comparison between the present study and the study of Wagner and Wendelin [18] is shown in Table 5.1.

Table 5. 1. Validation of the current study with the study of Wagner and Wendelin [18].

	Heliostat count	$\eta_{shading}$ (%)	$\eta_{cosine}$ (%)	$\eta_{blocking}$ (%)	$\eta_{intercept}$ (%)	$\eta_{absorption}$ (%)
Present Study	8731	100	80.31	98.8	95.19	94
Wagner and Wendelin [10]	8945	100	80.6	99	96	94

#### 5.2 Study of Ashikuzzaman and Adnan

To get further confirmation of the validity of the present study, another work of Ashikuzzaman and Adnan [24] has been regenerated. They calculated the optical efficiency of Crescent Dunes [38] CSP at various times of the day and year at the barren land of Tonopah, Nevada.

### 5.3 Generation of layout

To regenerate the layout, a C program is developed and run in order to get the cartesian coordinates of the heliostats. The text layout file is imported in SolarPILOT, and simulation has been performed afterwards. The C program is as follows-

```
#include <stdio.h>
#include <math.h>

int main()
{
    int i,j,r=150,z=0,n;
    float p, pi=3.1416,theta, deltheta, x,y, thetarev=0;

    for(i=1; i<=45; i++)
    {
        p=2*pi*r;
        n=p/20;
        deltheta=360/n;
        theta=thetarev;
        for(j=1;j<n;j++)
        {
            if (r<=210)
            {
                if (theta<=23||157<=theta<=203,337<=theta)
                {
                    x=r*cos(theta);
                    y=r*sin(theta);
                    printf("%f , %f \n", x,y);
                }
            }
            else if (r<=280)
            {
                if (theta<=18||162<=theta<=198,342<=theta)
                {
                    x=r*cos(theta);
                    y=r*sin(theta);
                    printf("%f , %f \n", x,y);
                }
            }
            else
            {
                if (theta<=15||165<=theta<=195,345<=theta)
                {
                    x=r*cos(theta);
                    y=r*sin(theta);
                    printf("%f , %f \n", x,y);
                }
            }
            theta=deltheta+theta;
        }
        if(i<5)
```

```

printf("%d \n", z);
else
{
    z=z+10;
    printf("%d \n", z);
}/*
r=r+10;
if(i % 2 == 0)
thetaprev=deltheta/2;
else
thetaprev=0;
}
}

```

$r$  and  $\theta$  in this program, define the distance and radial angle of any heliostat  $j$  respectively. The portion of  $z$  in the program remains commented when validating (it has purpose while generating a 3D layout).

#### 5.4 Validation

The layout is shown in Figure 5.1(a) and the comparison is illustrated in Figure 5.1(b). It can be confirmed from the figure that present study almost identically regenerated the findings of Ashikuzzaman and Adnan [24].

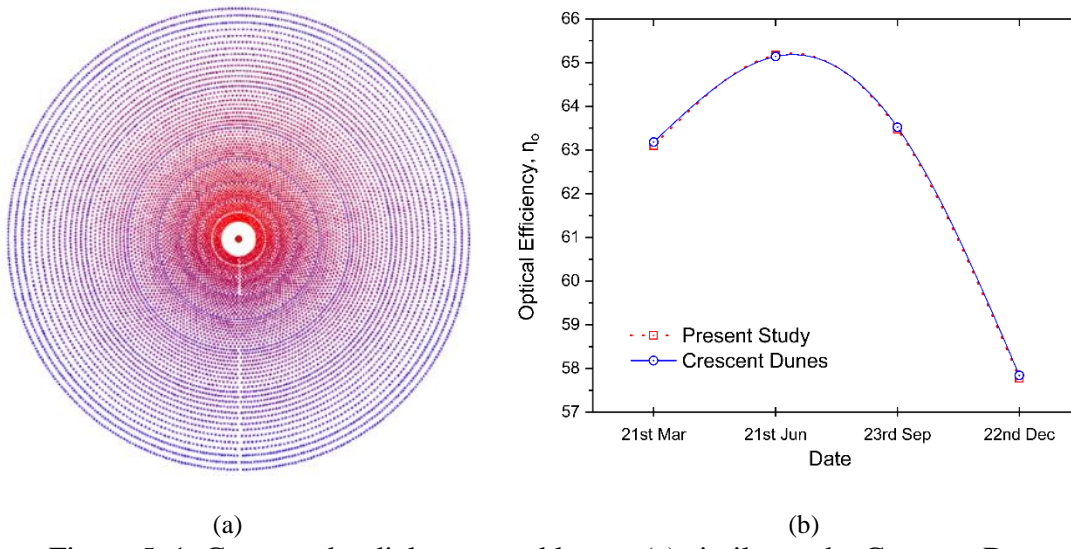


Figure 5. 1. Generated radial staggered layout (a) similar to the Crescent Dunes, Tonopah; and the optical efficiency (b) at 10am, for four specific days of the year for both the original and the generated similar layout on SolarPILOT.

# **Chapter 6**

## **Result and Discussion**

### **6.1 Potential of inclined V-shape**

The first portion of the present study investigates the potentiality of inclined V-shape layout in the hilly areas for three different locations of USA. The areas are chosen based on the utility and the solar irradiation of the places. First of all, to visualize the capability of solar radiation absorption of the receiver, flux profile and blocking efficiency are generated for three different time of the day, at equinoxes and solstices for all three locations and displayed in Figure 9 to 14. In the morning (9:00) and the afternoon (15:00), central receiver extracts irradiation flux at the cylindrical curves facing the heliostat fields, and the flux is a bit higher at the parts in the direction of sun and leaves a trapezoidal projection on the cylindrical surface of the receiver. At noon the sun is near the meridian, central receiver receives the majority of the irradiation.

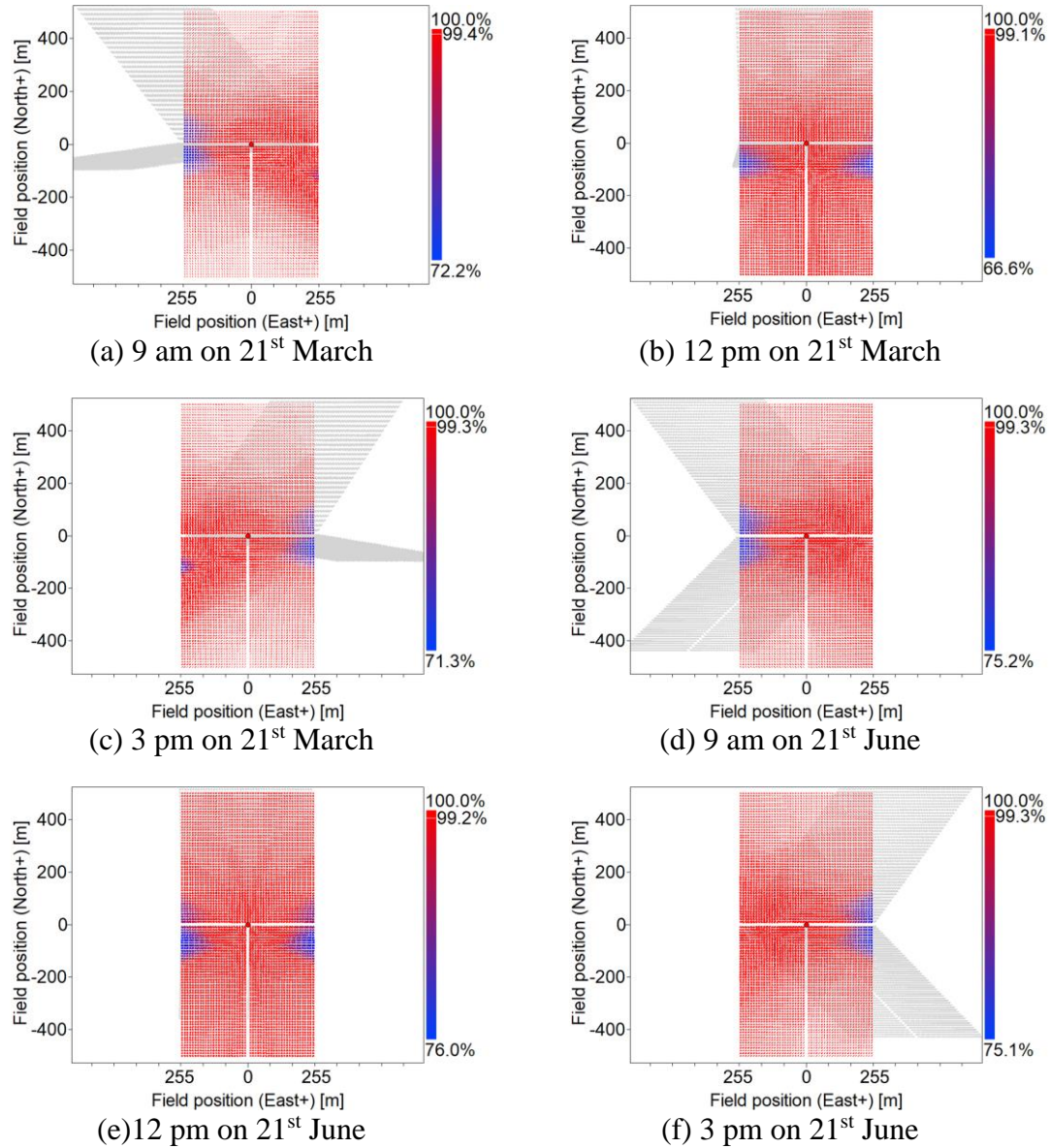
### **6.2 Location 1**

V-shape layout is simulated for optical efficiency comprising of cosine efficiency, blocking efficiency, shadowing efficiency and image intercept efficiency. The receiver flux profile is also observed throughout the year to get a clear perspective of the potential of this location as a H-CSP site.

#### **6.2.1 Blocking Efficiency**

Improving blocking efficiency stands out as a key objective in this investigation. In Figure 6.1(a) – (l), the field layout's performance is illustrated across the entire year and as daytime progresses. Given that this efficiency is contingent on the sun's position, it is evident that fewer heliostats are affected by blocking when the sun is inclined to the north by several degrees. In simpler terms, blocking efficiency is notably greater in months like March and September compared to June. Despite the fact that the intensity of the blocking factor is

more pronounced in the morning and afternoon than at noon, this is attributed to the high inclination angle of the layout, such as  $45^\circ$ . Importantly, this trend remains consistent throughout the entire year.



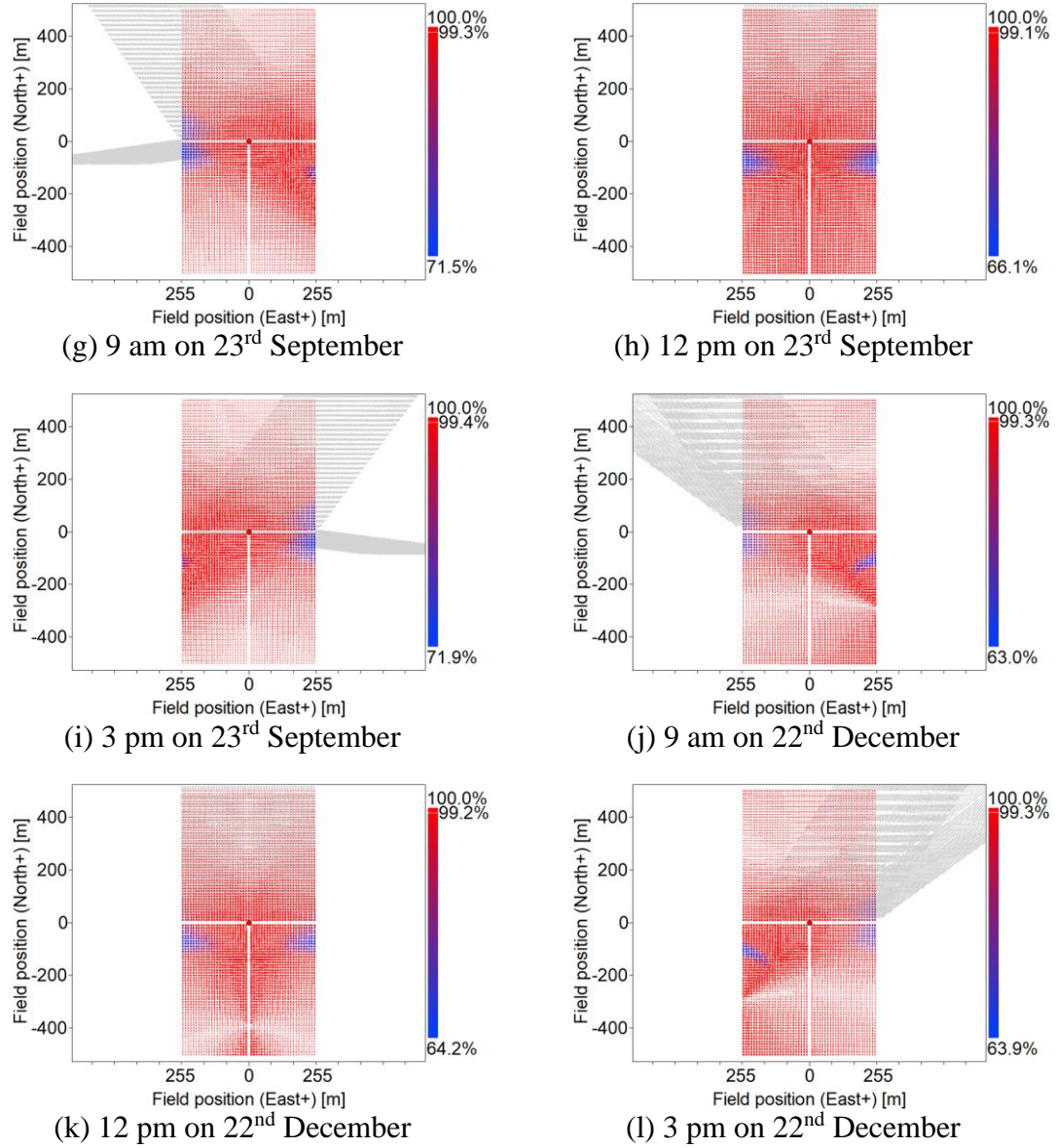


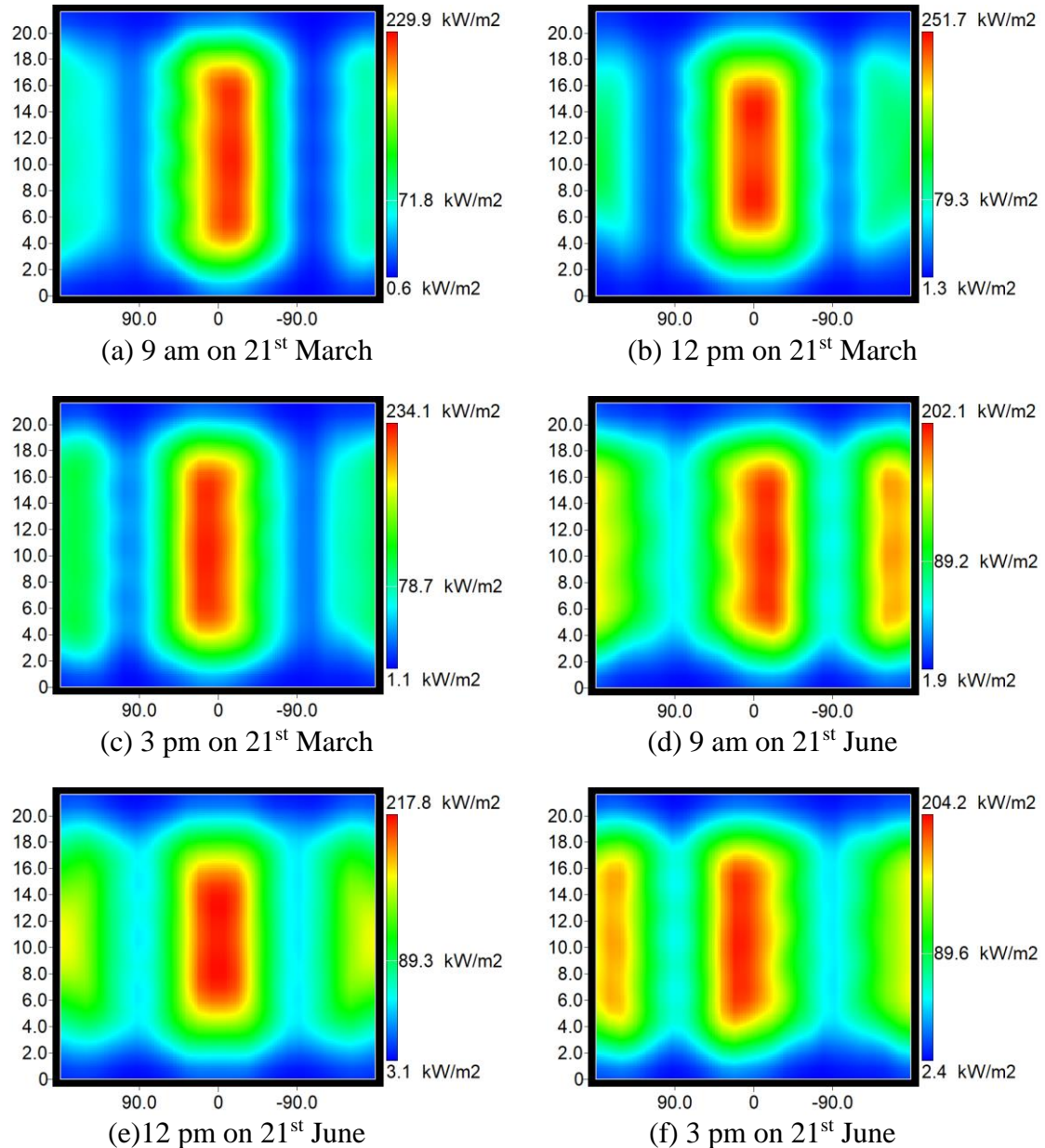
Figure 6. 1. The blocking efficiency of the layout at different times and dates of the year at Location 1.

### 6.2.2 Receiver Flux profile

Figure 6.2(a) – (l) shows the receiver flux profile for the layout at Location 1. Similar to the blocking efficiency study, receiver flux is observed throughout the year for different times of the day. Receiver having a cylindrical surface can be shown as a flat surface in 2D. And the layout having two wings spread at north and south it is obvious that the flux intensity will peak in the respective side. Surprisingly, the highest intensity peaks in the

## Chapter 6

months of March, September, and December to more than  $250 \text{ kW/m}^2$  rather than in June. This must create confusion, but to clarify the total reflected irradiation incident on the receiver is still high in the month of June, shown in Figure 6.2(d) - (f).



## Chapter 6

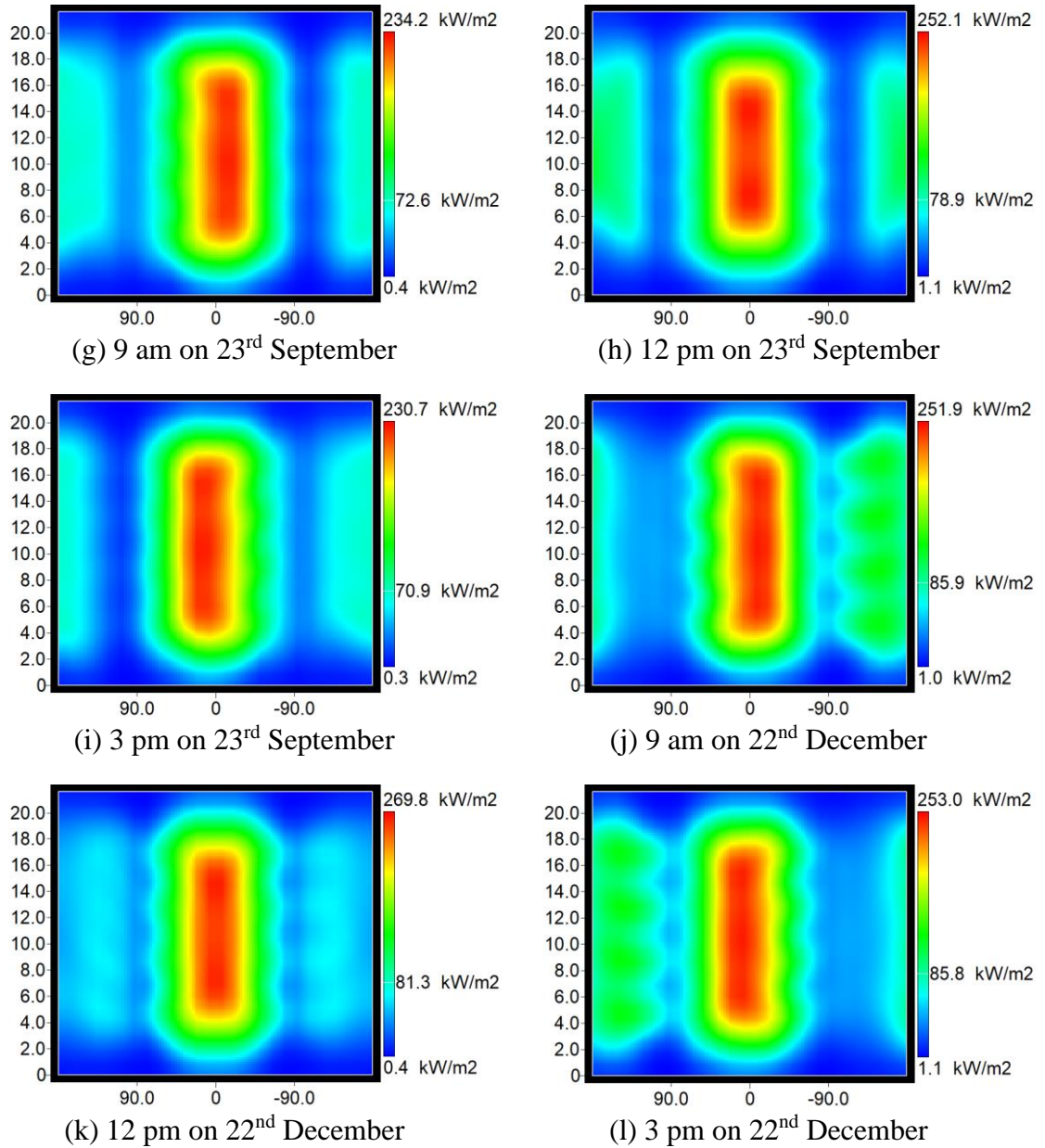


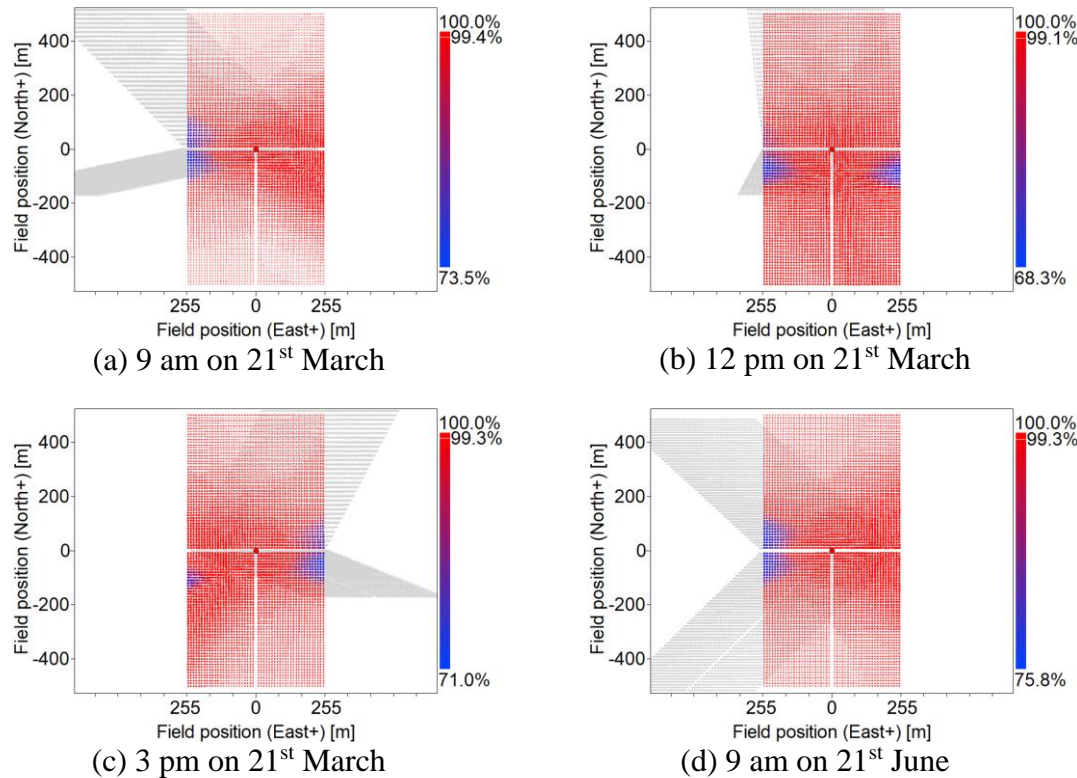
Figure 6. 2. The receiver flux profile at different time and dates of the year at Location 1. (x-axis represents the angular position of the cylindrical receiver surface, where  $0^\circ$  indicating to the North,  $+90^\circ$  the East,  $-90^\circ$  the west and  $\pm 180$  indicates the south; y-axis represents the height of the receiver tower).

### 6.3 Location 2

Not unlike location 1, the V-shaped layout is modeled to assess optical efficiency, for location 2 as well. Additionally, the flux profile at the receiver is analyzed for location 2 too throughout the year to gain insights into the suitability of this location as a H-CSP site.

#### 6.3.1 Blocking Efficiency

A similar process to Location 1 is performed for Location 2 to investigate the performance of blocking factor. Figure 6.3(a) – (l) depicts the performance of the field layout throughout the whole year and as the daytime progresses. Since, this factor solely depends on the position of the sun here too, it is observed that the number of heliostats experiencing blocking is much less, when the sun is inclined to the north by some degrees, exhibiting a similar result throughout the year as location 1.



## Chapter 6

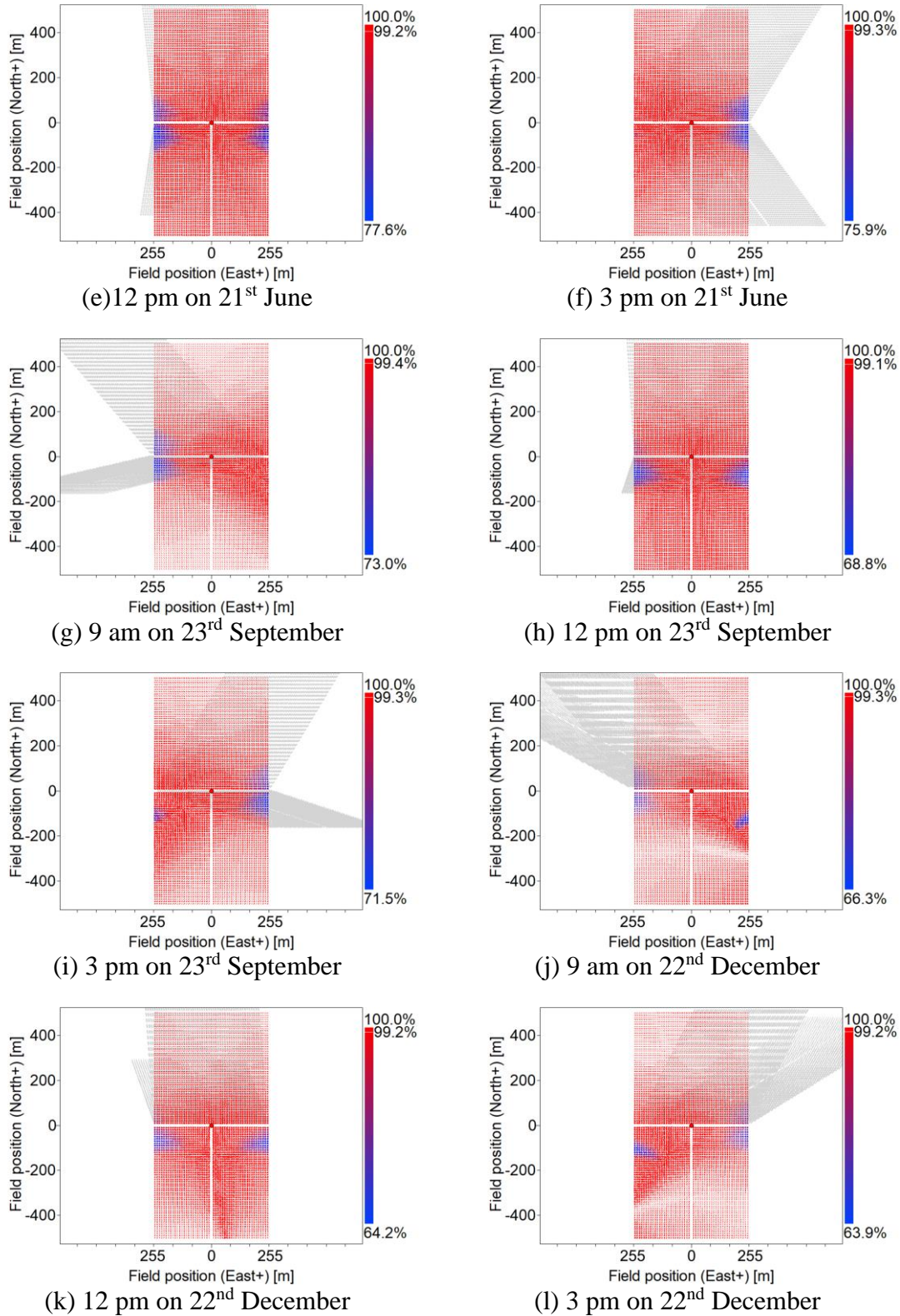
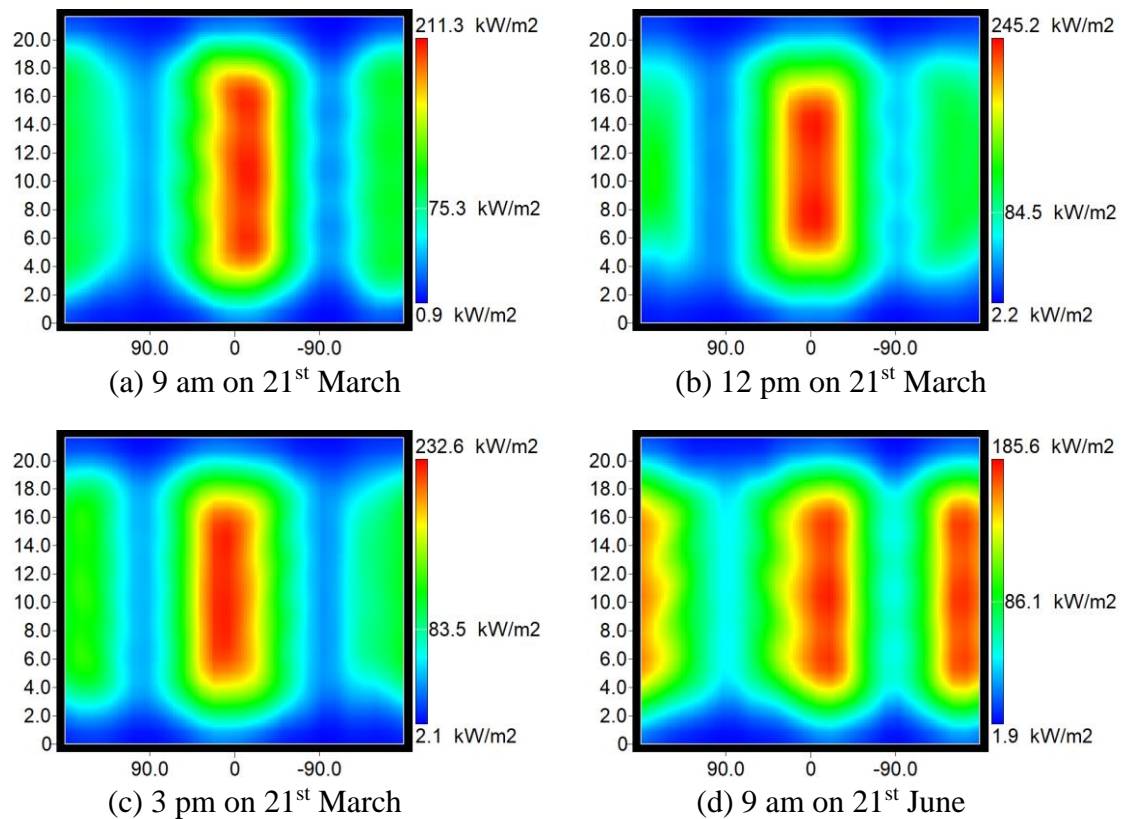


Figure 6. 3. The blocking efficiency of the layout at different time and dates of the year at Location 2.

### 6.3.2 Receiver Flux profile

Figure 6.4(a) – (l) illustrates the receiver flux profile for the layout at Location 1. Much like the examination of receiver flux profile for location 1, the study here for location 2 extends throughout the entire year, considering various times of the day. Visualizing the receiver with a cylindrical surface as a flat 2D entity. Interestingly, the highest intensity peaks occur in the months of March, September, and December, similar to location 1 trend, however surpassing  $245 \text{ kW/m}^2$  is less than that of location 1, contrary to expectations of a peak in June. Similar to location 1, the total reflected irradiation incident on the receiver remains consistently high in the month of June, as depicted in Figure 6.4(d) - (f).



## Chapter 6

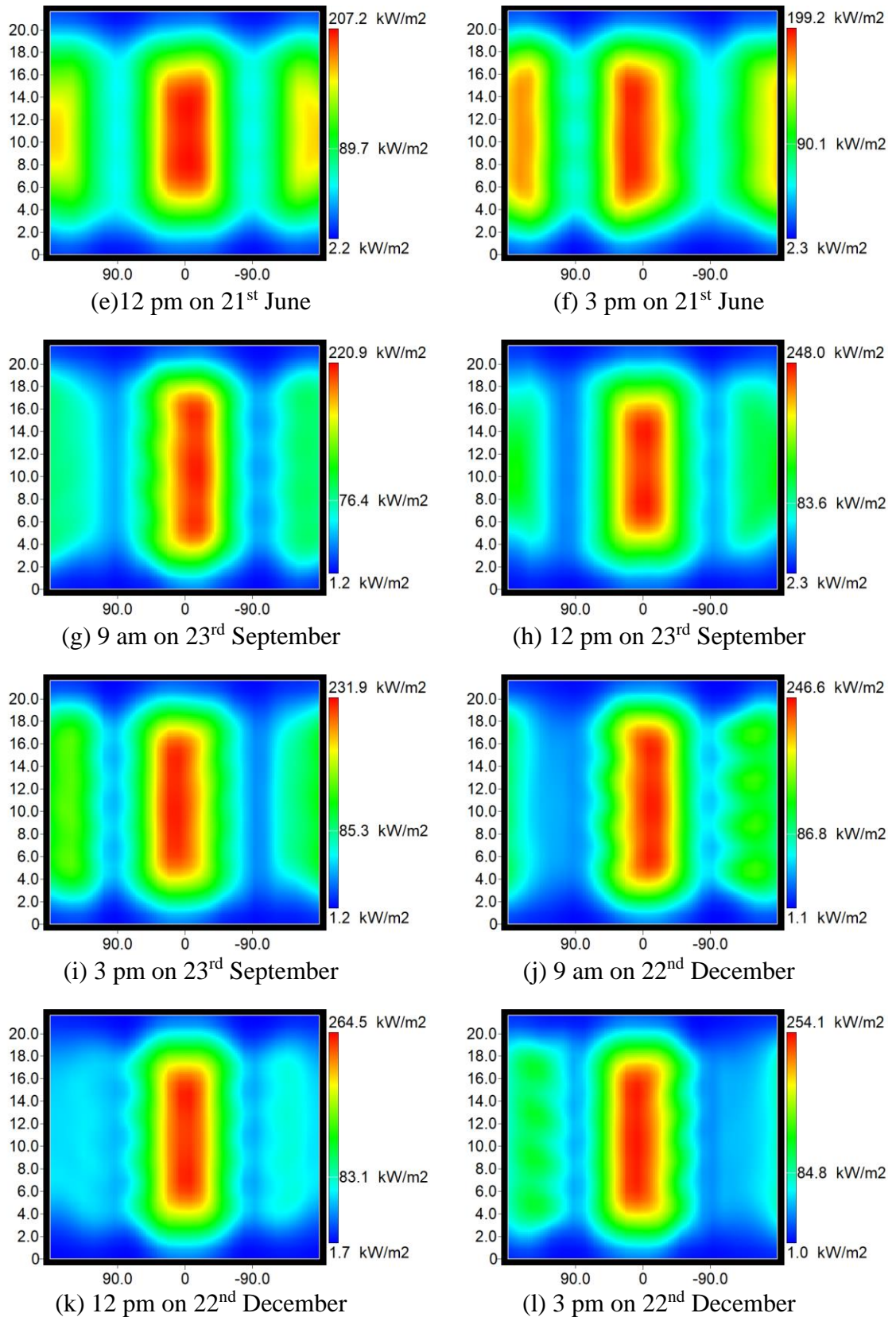


Figure 6.4. The receiver flux profile at different time and dates of the year at Location 2.

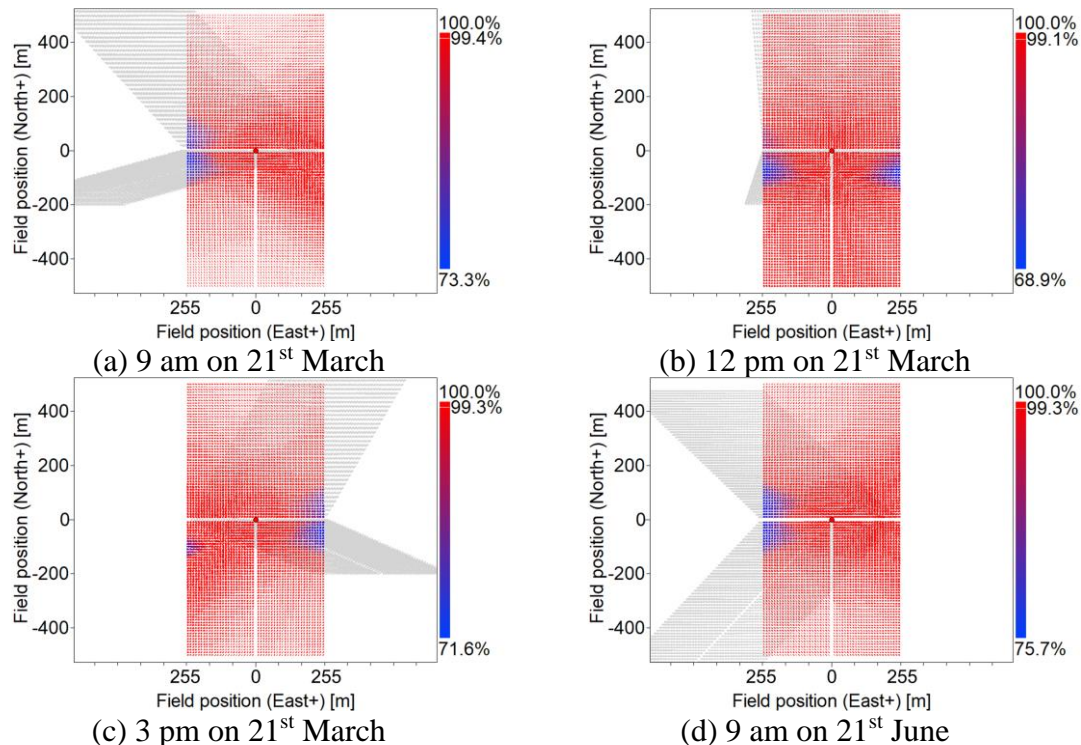
(x-axis represents the angular position of the cylindrical receiver surface, where  $0^\circ$  indicating to the North,  $+90^\circ$  the East,  $-90^\circ$  the west and  $\pm 180$  indicates the south; y-axis represents the height of the receiver tower).

## 6.4 Location 3

In a similar manner to the other locations, an assessment of optical efficiency is conducted for a V-shaped layout. Furthermore, the receiver flux profile is monitored year-round to ascertain the potential of this site for H-CSP applications.

### 6.4.1 Blocking Efficiency

Figure 6.5(a) – (l) visually represents the performance of the field layout across the entirety of the year and its evolution throughout the course of each day. Not unlike the other two locations, blocking efficiency exhibits a considerable upswing during months like March and September, contrasting with its performance in June. It's noteworthy that this pattern remains consistently observable throughout the entire annual cycle.



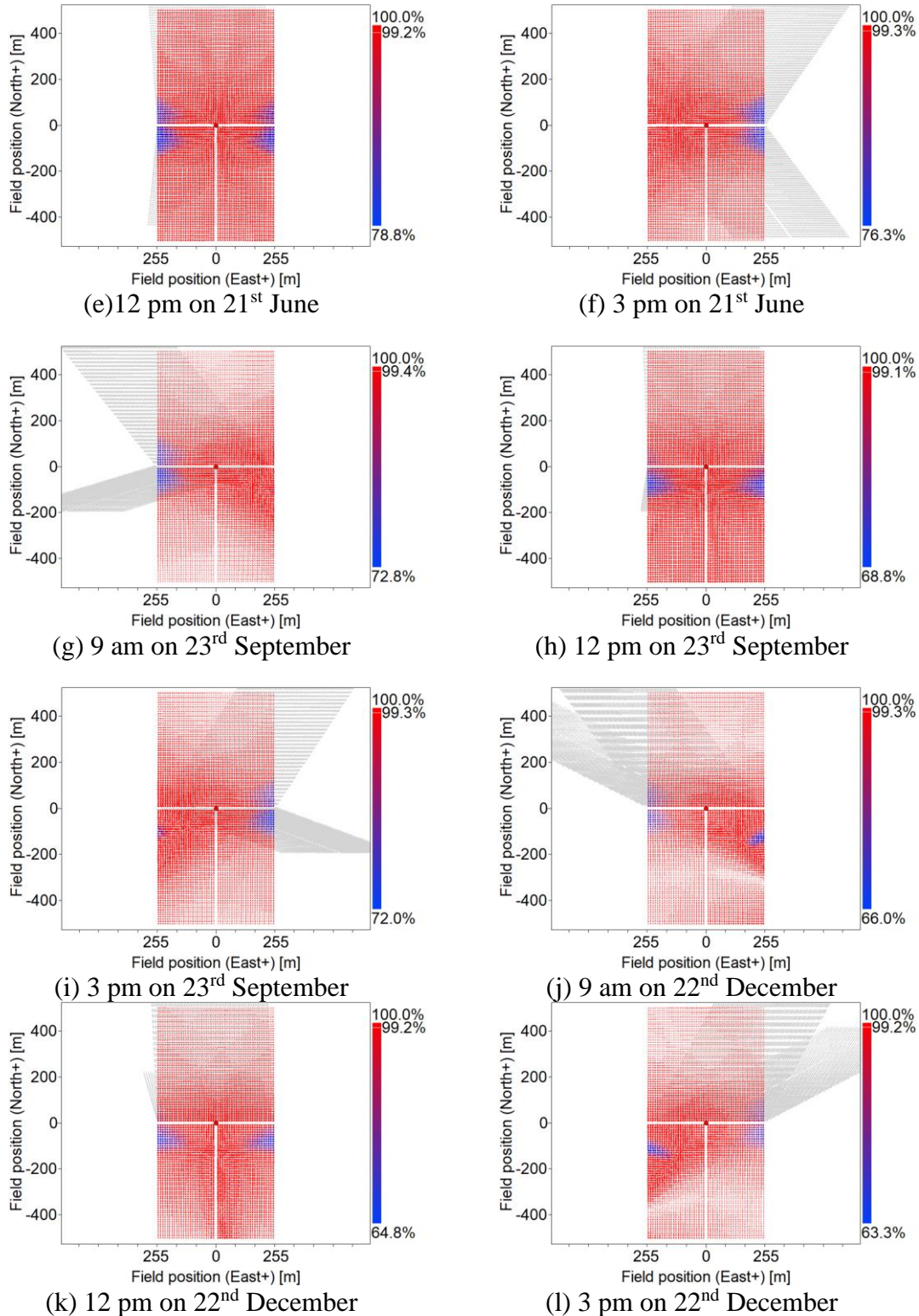
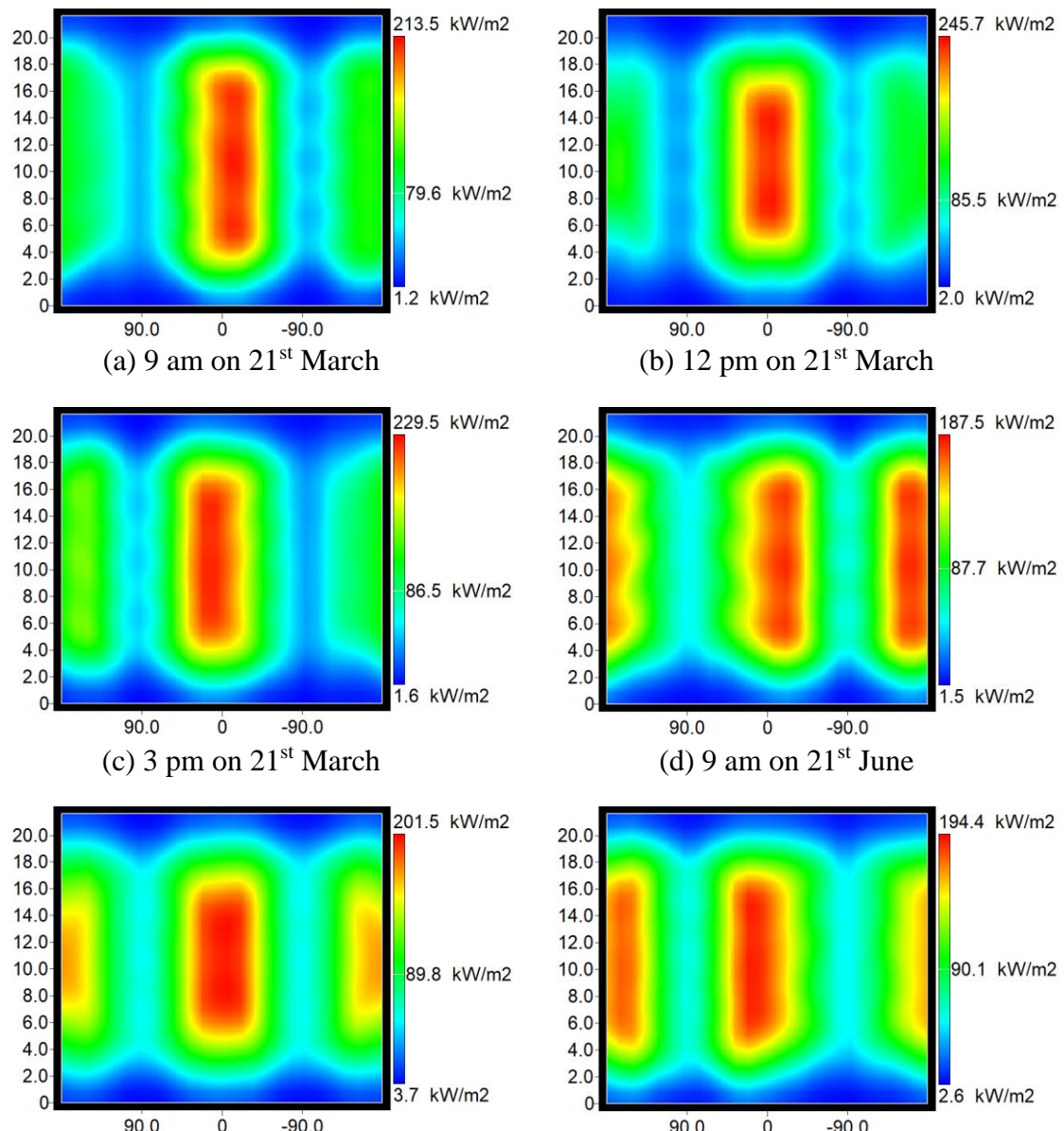


Figure 6. 5. The blocking efficiency of the layout at different time and dates of the year at Location 3.

### 6.4.2 Receiver Flux profile

Displayed in Figure 6.6(a) – (l) is the profile of receiver flux for the layout situated at Location 3. Mirroring the methodology applied in studying the receiver flux profile of other locations, this investigation delves into the receiver flux dynamics across all seasons and various times of the day. With no surprise, like other locations, the zenith of intensity manifests in the months of March, September, and December here too, surpassing an impressive  $248 \text{ kW/m}^2$ , less than location 1 however and with a hike than location 2, defying conventional expectations of a peak in June.



## Chapter 6

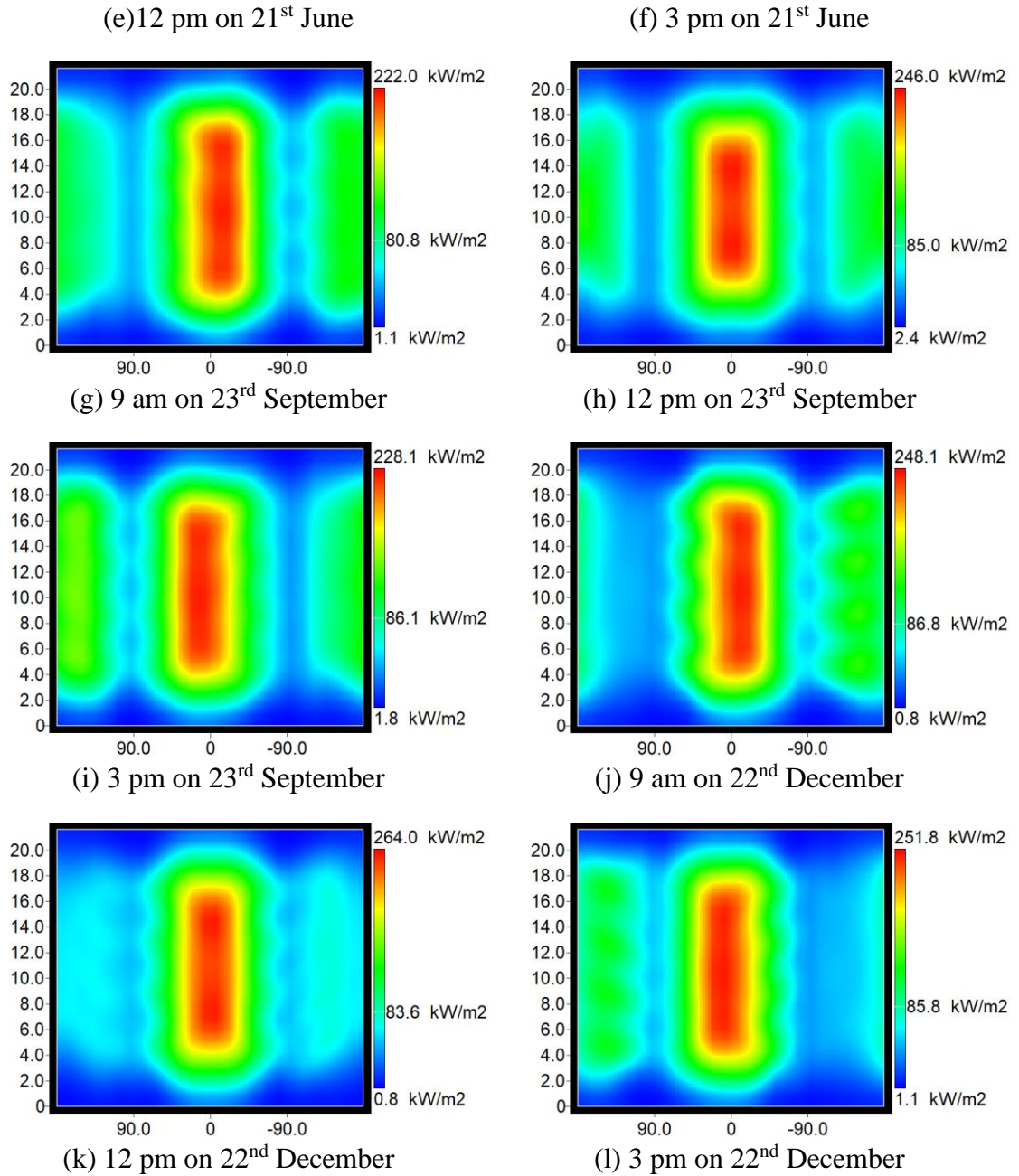


Figure 6.6. The receiver flux profile at different time and dates of the year at Location 3. (x-axis represents the angular position of the cylindrical receiver surface, where  $0^\circ$  indicating to the North,  $+90^\circ$  the East,  $-90^\circ$  the west and  $\pm 180$  indicates the south; y-axis represents the height of the receiver tower).

## 6.5 Efficiency data analysis

Further investigation is continued to evaluate the associated efficiencies of optical efficiency of the places for different dates of the year and different time of the day and shown in Table 6.1 – 6.3. At Location 1, optical efficiency ranges from approximately 61% to 66%. The reason is cosine efficiency peaks on 21<sup>st</sup> June; the simulation result shows that peak cosine efficiency is at 9:00 in the morning and 15:00 in the afternoon and the least at winter solstice. Blocking and Intercept efficiency are almost same all around the year. At Location 2, optical efficiency ranges from approximately 62% to 67% since cosine efficiency peaks in the summer solstice and the result trend is similar to that of Location 1. Again, a similar trend is observed for Location 3, in cosine, blocking and intercept efficiency and that is why the optical efficiency ranges from approximately 62.5% to 67%. It is observed from the figures that, even though overall optical efficiency is better throughout the year in Location 3 than the others, all three locations are magnificently efficient and comparable to each other.

### 6.5.1 Location 1

In Blue canyon AP, CA, USA, cosine efficiency peaks in the summer solstice (21<sup>st</sup> June) but not at 12 pm; the simulation data shows that peak cosine efficiency is at 9 am in the morning and 3 pm in the afternoon. Cosine efficiency is the least in winter solstice. Blocking efficiency is almost same all around the year. Intercept efficiency is also almost unchanged throughout the year. All the individual efficiencies combined with the Optical Efficiency range from approximately 61% to 66%.

Table 6. 1. Individual Efficiencies in Location 1 (Blue Canyon Ap, California, USA)

<b>LOCATION 1</b>	<b>Time of Day</b>	<b>Cosine Efficiency</b>	<b>Blocking Efficiency</b>	<b>Shading Efficiency</b>	<b>Intercept Efficiency</b>	<b>Optical Efficiency</b>
21-Mar	9:00 AM	67.1	99.4	90.2	99.2	66.16
	12:00 PM	65.3	99.1	93.3	99.1	64.12
	3:00 PM	66.9	99.3	98.1	99.2	65.90
21-Jun	9:00 AM	68	99.3	100	99.2	66.98
	12:00 PM	67.4	98.9	100	99.1	66.05

## Chapter 6

		3:00 PM	68	99.3	100	99.2	66.98
23-Sep	9:00 AM	66.9	99.4	98.4	99.2	65.96	
	12:00 PM	65.2	99.1	92.8	99.1	64.03	
	3:00 PM	67	99.4	96.4	99.2	66.06	
22-Dec	9:00 AM	65.3	99.5	98.2	99.1	64.38	
	12:00 PM	62.6	99.3	100	99	61.54	
	3:00 PM	65.6	99.5	98.5	99.1	64.68	

### 6.5.2 Location 2

In Deer Valley Phoenix, AZ, USA, cosine efficiency peaks in the summer solstice (21<sup>st</sup> June); the simulation data shows that peak cosine efficiency is at 9 am in the morning for 68.1%. Cosine efficiency is the least in winter solstice. Blocking efficiency is almost same all around the year. Intercept efficiency is also almost unchanged throughout the year. All the individual efficiencies combine the Optical Efficiency range from approximately 62% to 67%.

Table 6. 2. Individual Efficiencies in Location 2 (Deer Valley Phoenix, Arizona, USA)

LOCATION 2	Time of Day	Cosine Efficiency	Blocking Efficiency	Shading Efficiency	Intercept Efficiency	Optical Efficiency
21-Mar	9:00 AM	67.6	99.4	85.8	99.2	66.65
	12:00 PM	66	99.1	100	99.1	64.81
	3:00 PM	66.9	99.3	94.4	99.2	65.90
21-Jun	9:00 AM	68.1	99.3	100	99.2	67.08
	12:00 PM	67.7	98.9	100	99.1	66.35
	3:00 PM	68	99.2	100	99.1	66.84
23-Sep	9:00 AM	67.5	99.4	92.7	99.2	66.55
	12:00 PM	65.9	99.1	100	99.1	64.71
	3:00 PM	67	99.3	96.8	99.2	65.99
22-Dec	9:00 AM	65.9	99.5	96.2	99.2	65.04
	12:00 PM	63	99.3	99.5	99.1	61.99
	3:00 PM	64.8	99.4	99.9	99.1	63.83

### 6.5.3 Location 3

In Lufkin, TX, USA, cosine efficiency peaks in the summer solstice (21<sup>st</sup> June); the simulation data shows that peak cosine efficiency is at 9 am in the morning and 3 pm in the afternoon for 68%. Cosine efficiency is the least in winter solstice. Comparing Table 6.3 with Table 6.1 and 6.2, it is observed that overall cosine efficiency all around the year is a bit better in this location for this layout. Blocking efficiency is almost same all around the year. Intercept efficiency is also almost unchanged throughout the year. All the individual efficiencies combine the Optical Efficiency range from approximately 62.5% to 67%.

Table 6. 3. Individual Efficiencies in Location 3 (Lufkin, Texas, USA)

LOCATION 3	Time of Day	Cosine Efficiency	Blocking Efficiency	Shading Efficiency	Intercept Efficiency	Optical Efficiency
21-Mar	9:00 AM	67.6	99.4	95.3	99.2	66.65
	12:00 PM	66.2	99	100	99.1	64.94
	3:00 PM	67.4	99.3	97.4	99.2	66.39
21-Jun	9:00 AM	68	99.3	100	99.2	66.98
	12:00 PM	67.8	98.9	100	99.1	66.45
	3:00 PM	68	99.2	100	99.2	66.91
23-Sep	9:00 AM	67.5	99.4	99.6	99.2	66.55
	12:00 PM	66.2	99	100	99.1	64.94
	3:00 PM	67.2	99.3	98.4	99.2	66.19
22-Dec	9:00 AM	65.8	99.4	97.5	99.1	64.81
	12:00 PM	63.3	99.3	98	99.2	62.35
	3:00 PM	65.1	99.4	99.5	99.1	64.12

### 6.6 Optical Efficiency analysis of three locations

The variation of optical efficiency along with the time of the day is quite unorthodox shown in Figure 6.7. The trend shows that it has higher value in the morning and the afternoon

## Chapter 6

rather than at noon. The reason must be the geographical position of the locations; since this layout has inclined sides, with a latitude of around 31 to 39°N, the cosine efficiency is reduced at noon, resulting in less optical efficiency than the other times of the day. A notable positive point of this layout can be observed by comparing these results to a highly efficient radial staggered layout in Crescent Dunes [5]. In Crescent Dunes, it is seen that although it has high cosine efficiency (about 80%), however, the blocking efficiency falls down to around 92 to 96% and intercept efficiency falls down to 97 to around 98%. Here, the HCSP system developed in this study achieves blocking and intercept efficiency more than 99% in all the selected regions.

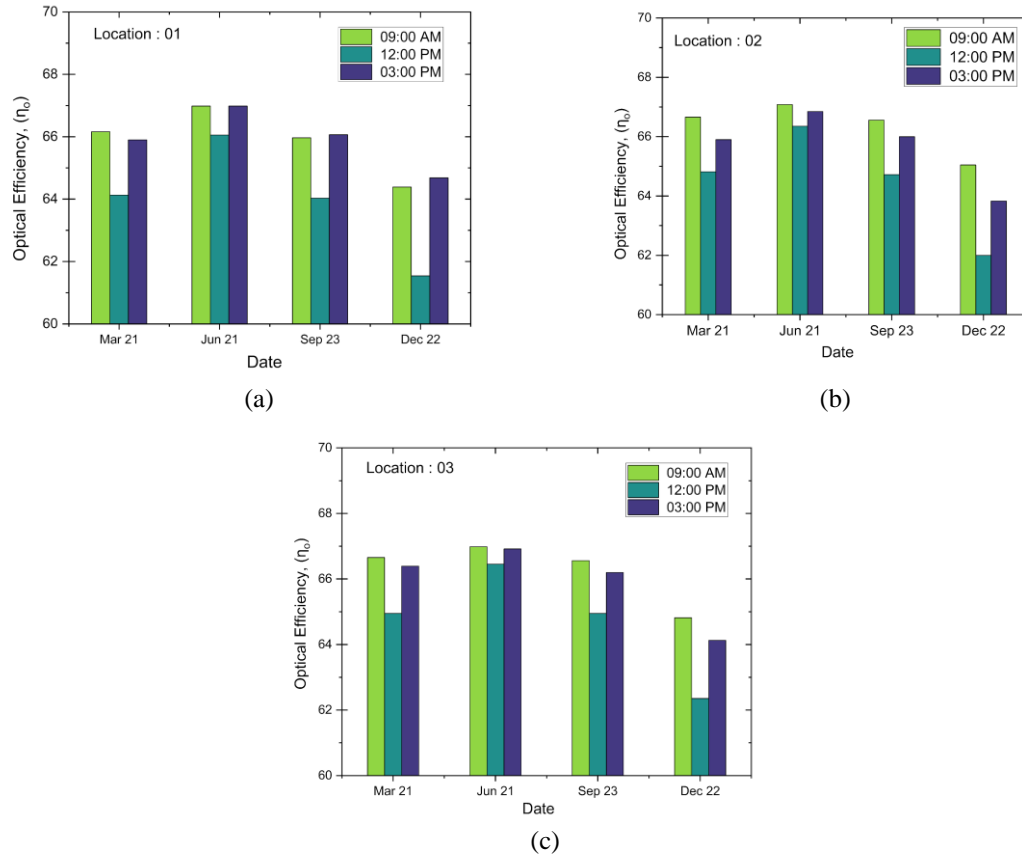


Figure 6.7. Variation of optical efficiency with the variation of time and date at (a) Location 1, (b) Location 2, and (c) Location 3.

### 6.7 Location 1 outperforming other locations

From the generated individual efficiency in Crescent Dunes [1] it is seen that although it has high cosine efficiency about 80% however the Blocking efficiency falls down to around

## Chapter 6

92 to 96% and Intercept efficiency falls down to 97 to around 98%. Here, the H-CSP system developed in this study achieves Blocking and Intercept efficiency more than 99% in all the selected regions. It can be observed that inclined surfaces with simple rectangular array of heliostats can generate higher efficiency than the highly efficient flat surface layouts like radial staggered [5] Hybrid 4 (Biomimetic in the north and Radial staggered in the south) [24]. Therefore, implementation of these layouts in the inclined surface may result in extraordinary level of efficiency. Looking at the receiver flux values, Location 1 has near to  $210 \text{ kW/m}^2$  or above throughout the year whereas the other two locations fall below to  $185 \text{ kW/m}^2$  or lower in some seasons of the year. Therefore, when planning for a potential site for a CSP besides the optical efficiency overall power generation throughout the year is necessary to be considered. And based on this point Location 1 becomes the most desirable location among the three.

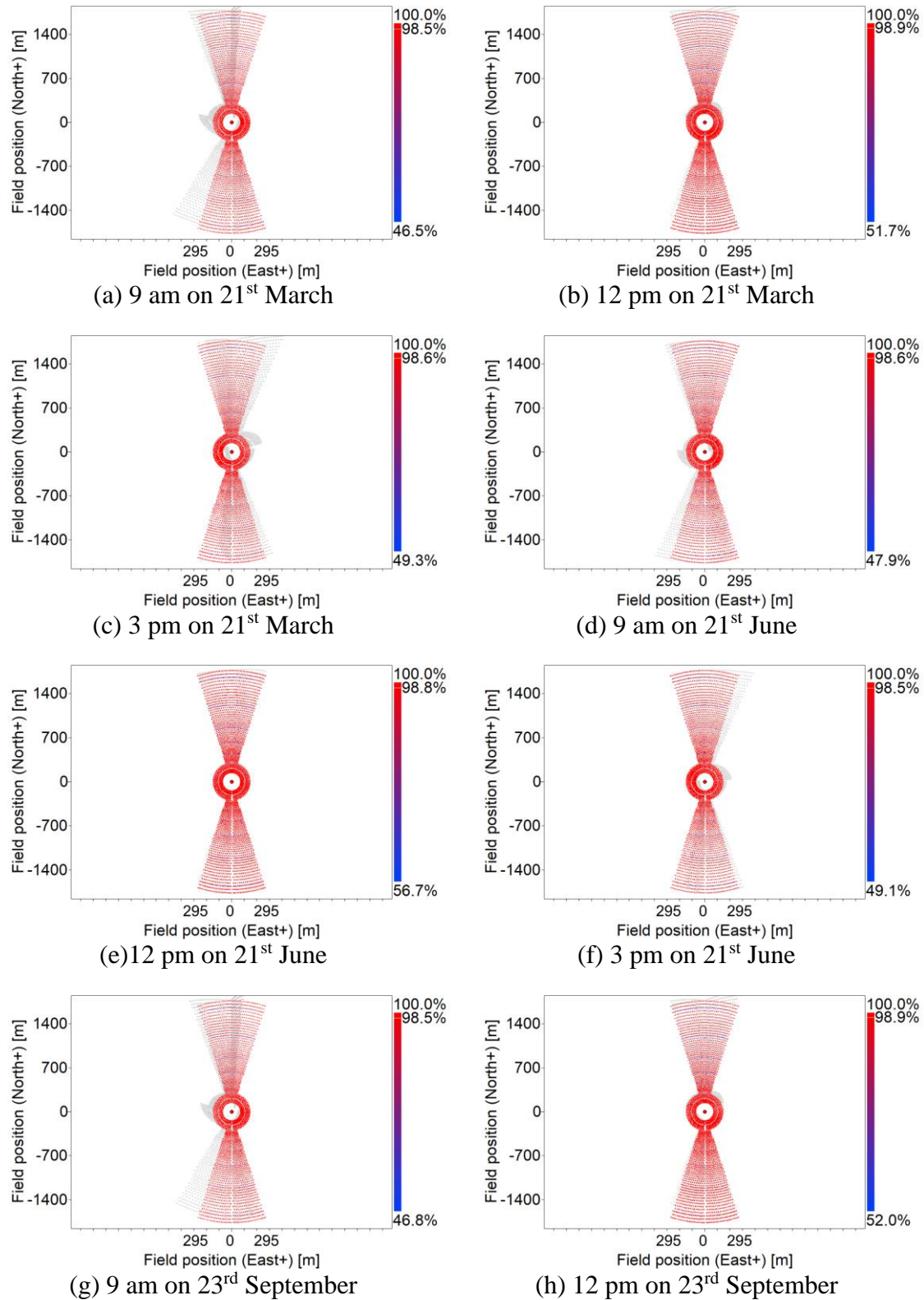
### **6.8 Site evaluation**

First Portion of the study states that inclined V-shape layouts have good potential to result in a higher optical efficiency. Therefore, to conduct the second portion of the study Location 1 has been prioritized due to its supreme performance over the other two and most practicality to build a H-CSP plant. Two selected sites based on their practicality with this study, has been simulated for optical efficiency and receiver flux profile as well.

#### **6.8.1 Blocking Efficiency at Site 1**

Some of the heliostat layers have been experiencing lower blocking efficiency at different times of the day or at different times of the year. This is because of the roughness of the real surface (steeper surfaces at some point and much flatten in some others) shown in Figure 6.8(a) – (l).

## Chapter 6



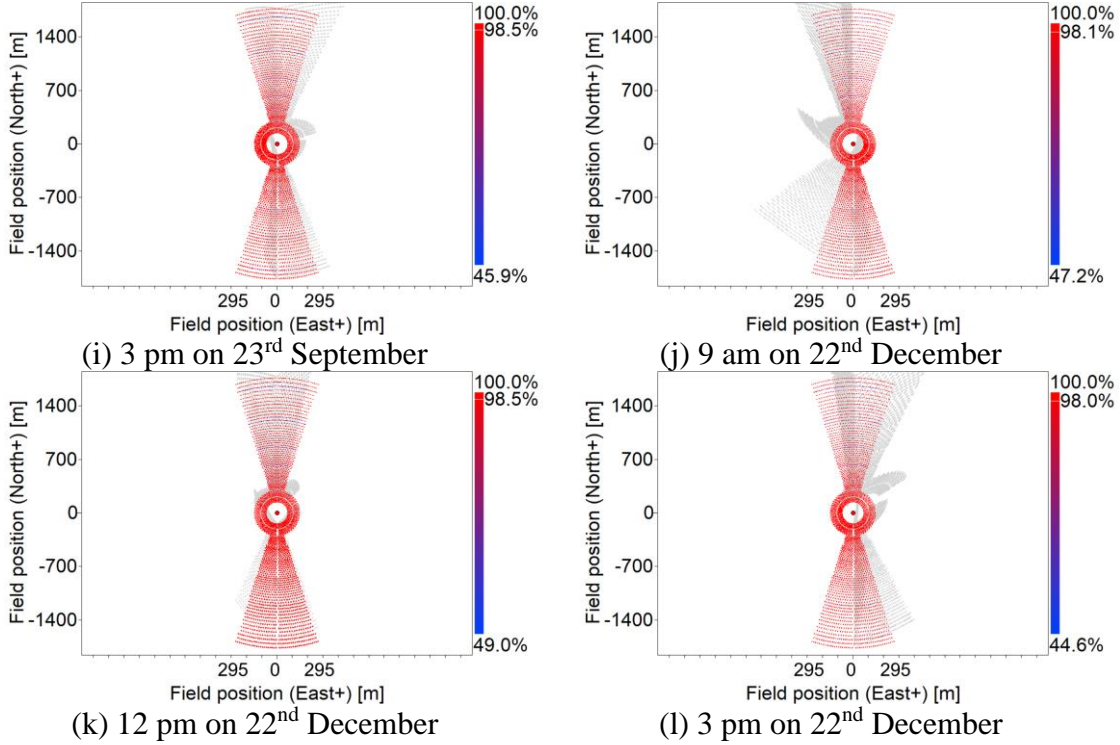
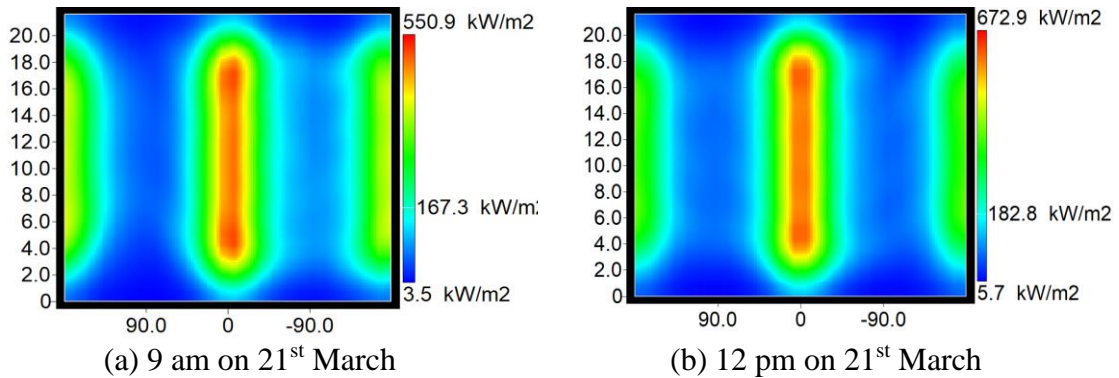


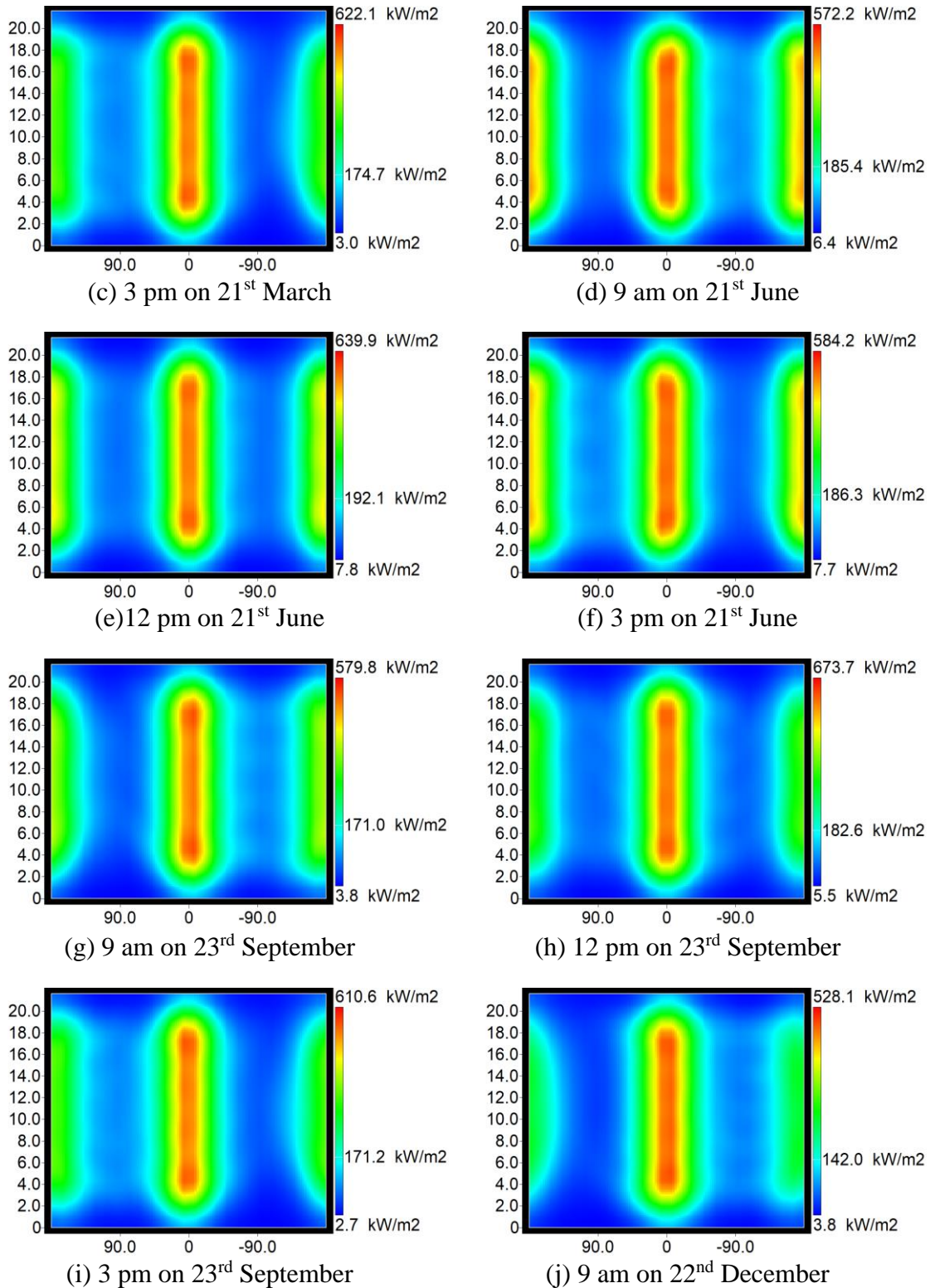
Figure 6.8. Blocking efficiency of the layout at different time and dates of the year at Site 1.

### 6.8.2 Receiver Flux profile at Site 1

Receiver Flux profile is much steeper for the receiver tower of site 1 shown in Figure 6.9(a) – (l). Another major thing that cannot go unnoticed is the much higher flux incident at the center. Here, incident flux goes up to  $672\text{ kW/m}^2$ , whereas plane V-shape layout could produce only up to  $220\text{ kW m}^2$ . This ultimately results in more incident flux at the receiver surface.



## Chapter 6



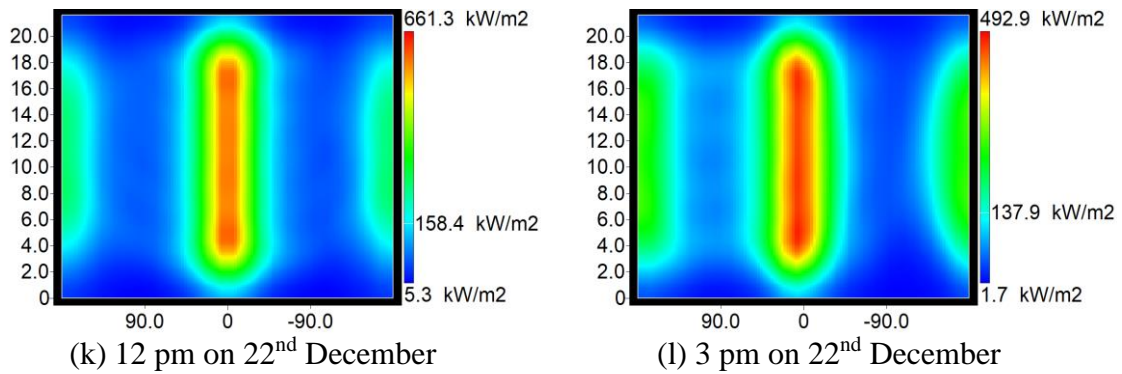


Figure 6. 9. The receiver flux profile at different time and dates of the year at Site 1. (x-axis represents the angular position of the cylindrical receiver surface, where  $0^\circ$  indicating to the North,  $+90^\circ$  the East,  $-90^\circ$  the west and  $\pm 180$  indicates the south; y-axis represents the height of the receiver tower).

### 6.8.3 Individual efficiency analysis

To evaluate the potential of the first site, associated efficiencies with the optical efficiency is evaluated like the previous manner. And here with no surprise the most eye-catching factor is higher cosine efficiency at noon shown in Table 6.4, which was quite unusual in the V-shape layout with inclination of  $45^\circ$ . The image intercept factor and the Shading efficiency is also slightly decreasing than the plane V-shape layout, which is logical. Since the average inclination has decreased to half, with the increased dimension of the heliostats these factors produce a little lower value than the plane one.

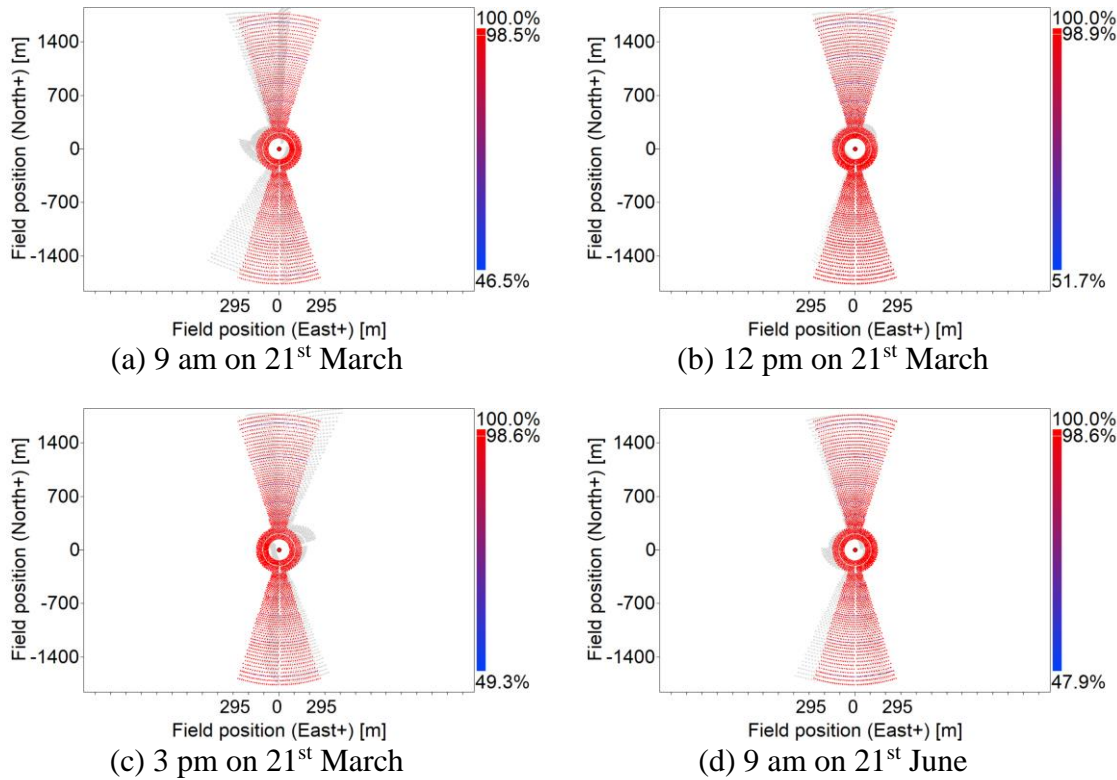
Table 6. 4. Individual Efficiencies in Site 1

SITE 1	Time of Day	Cosine Efficiency	Blocking Efficiency	Shading Efficiency	Intercept Efficiency	Optical Efficiency
21-Mar	9:00 AM	73.7	98.31	94.66	94.34	64.70
	12:00 PM	75.19	98.67	99.93	95.01	70.43
	3:00 PM	74.31	98.49	97.47	94.6	67.48
21-Jun	9:00 AM	76.81	98.59	99.38	95.03	71.51
	12:00 PM	78.56	98.78	100	95.4	74.03
	3:00 PM	76.95	98.56	99.65	95.08	71.85
23-Sep	9:00 AM	73.88	98.37	96.25	94.48	66.08
	12:00 PM	75.08	98.66	99.96	95	70.34

	3:00 PM	74.16	98.41	95.93	94.48	66.14
22-Dec	9:00 AM	68.71	97.45	87.95	93.45	55.03
	12:00 PM	68.21	97.93	97.11	94.24	61.13
	3:00 PM	66.8	97.52	87.87	94	53.80

#### 6.8.4 Blocking Efficiency for Site 2

A similar trend as Site 1 is noticed for the Site 2 as well. Although, Site 2 having a bit lesser average inclination result in a bit lesser individual efficiency. Almost similar performance to site 1 is given by the Site 2 in terms of cosine efficiency. Both the sites receive almost same solar irradiation however Site 2 having a lesser average inclination lowers cosine efficiency by a few points visually depicted in Figure 6.10(a) – (l).



## Chapter 6

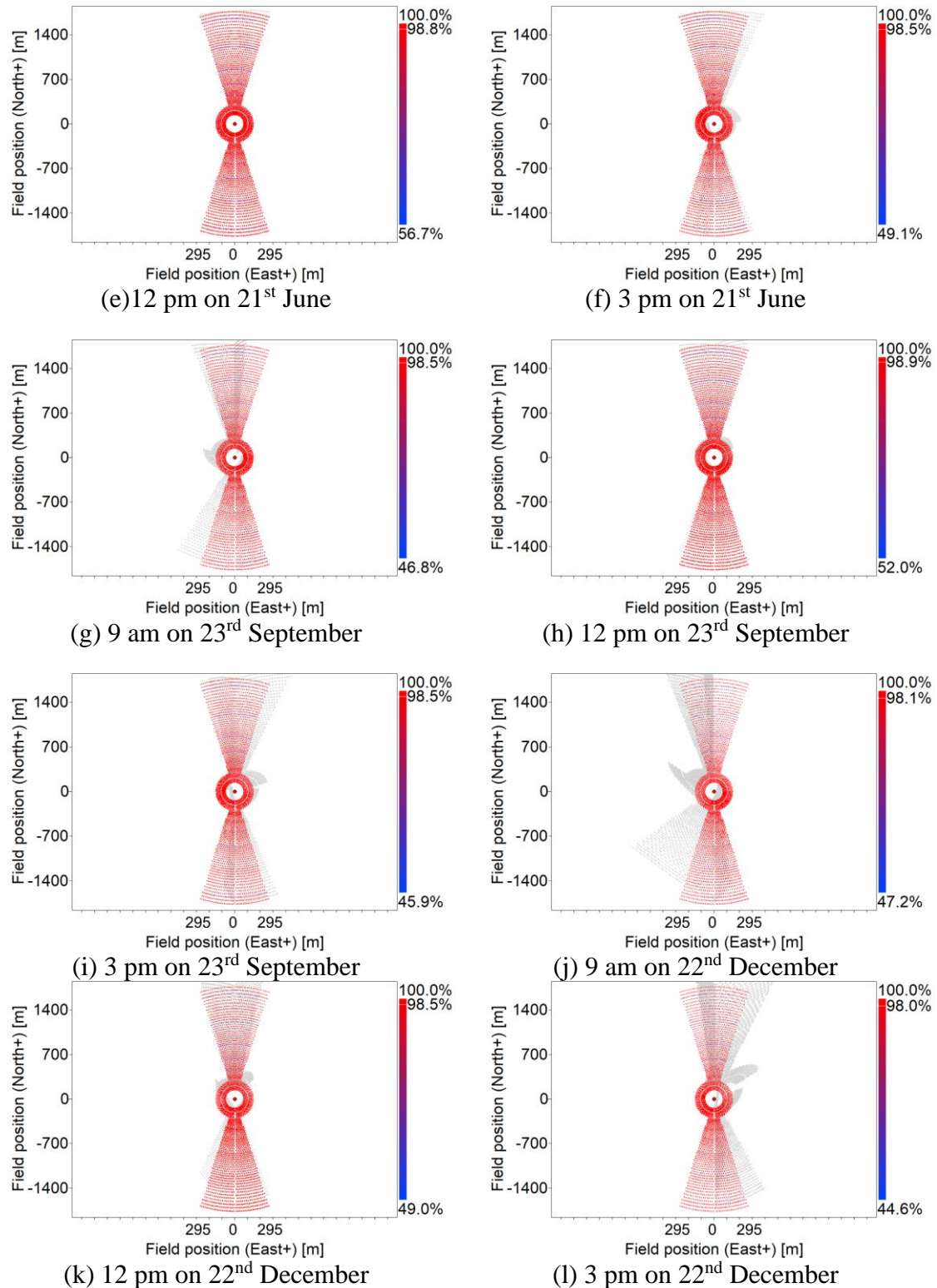
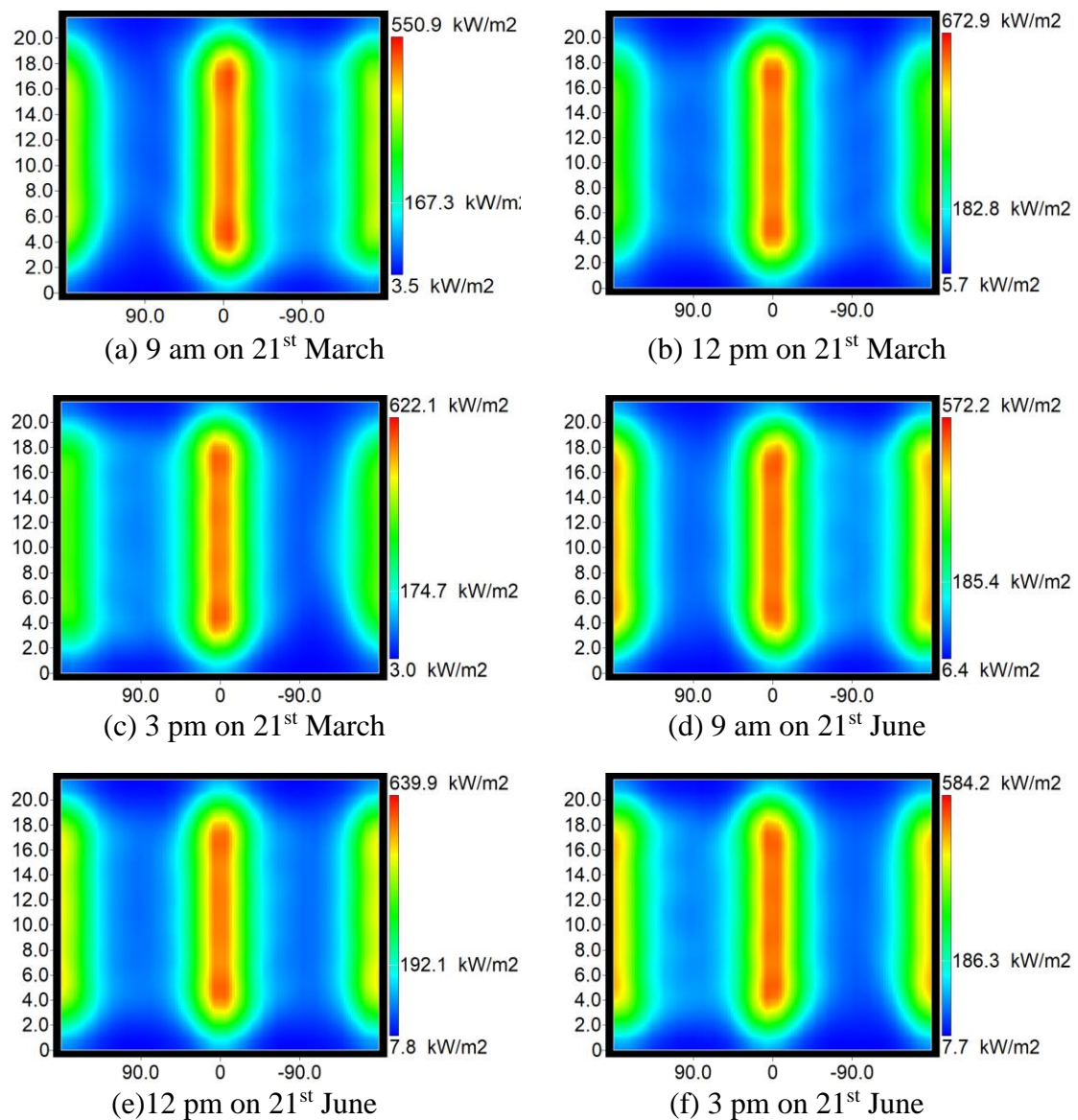


Figure 6.10. Blocking efficiency of the layout at different time and dates of the year at Site 2.

### 6.8.5 Receiver Flux profile for Site 2

Receiver Flux incident on the Receiver wall is almost the same as the Site 1. Both show a steeper profile at the center with a high incident flux shown in Figure 6.11(a) – (l). Although Site 2 has a bit lesser incident flux on the receiver wall than Site 1. This is because Site 2 is a bit inclined to the south-east to north-west axis, which is why it has some blocking tendency at some layers at some time of the day, mostly in March and December when Sun is more inclined to the center of the plant.



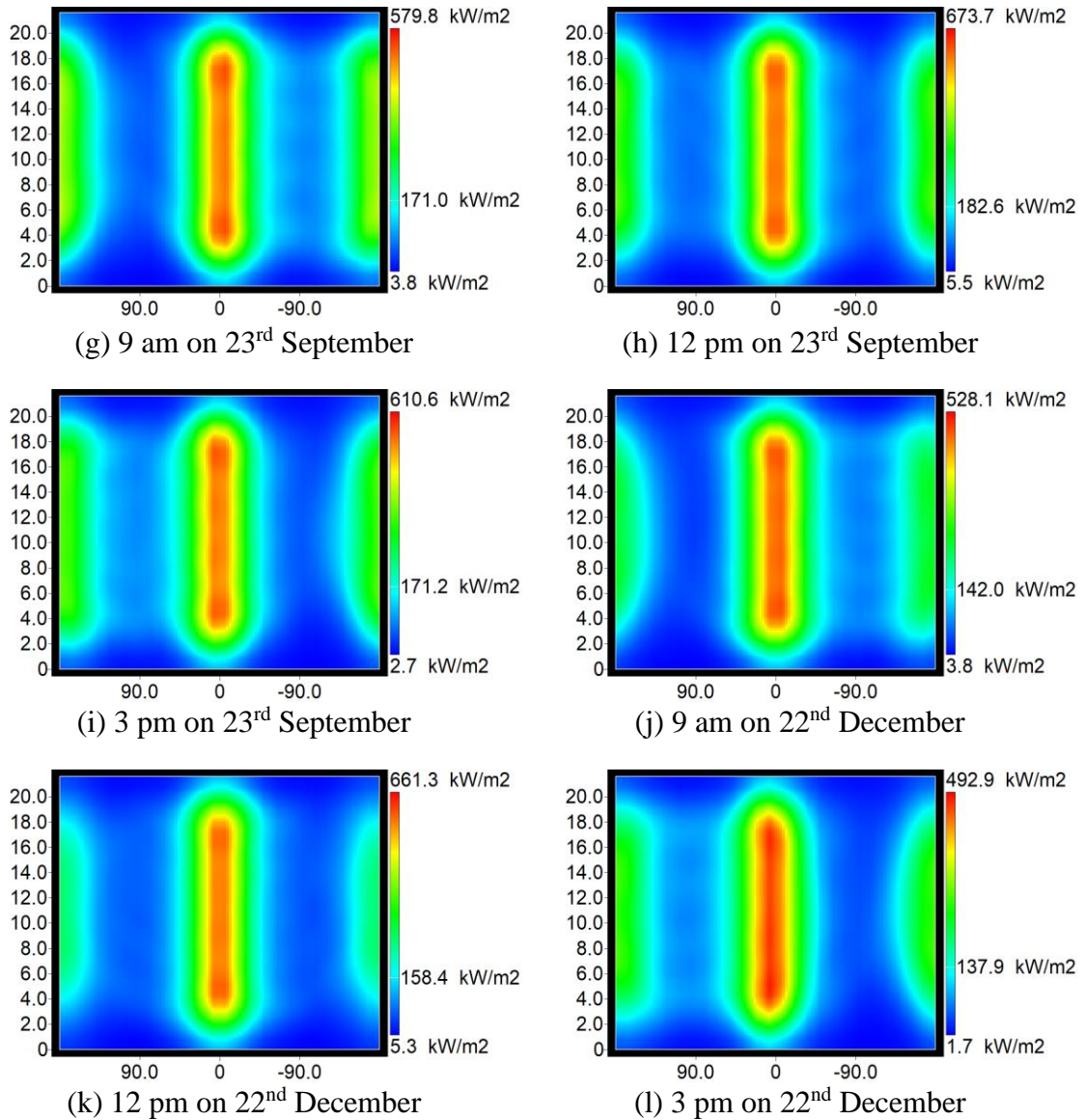


Figure 6. 11. The receiver flux profile at different time and dates of the year at Site 2. (x-axis represents the angular position of the cylindrical receiver surface, where  $0^\circ$  indicating to the North,  $+90^\circ$  the East,  $-90^\circ$  the west and  $\pm 180$  indicates the south; y-axis represents the height of the receiver tower).

### 6.8.6 Individual efficiency analysis for Site 2

Site 2 being less inclined than Site 1 and a bit tilted towards the south-east to north-west individual efficiencies addressed in Table 6.7, represents the fact. Therefore, it requires no words to justify that all the individual efficiencies result in a lesser value by a few points than those of the site 1.

Table 6. 5. Individual Efficiencies in Site 1.

SITE 1	Time of Day	Cosine Efficiency	Blocking Efficiency	Shading Efficiency	Intercept Efficiency	Optical Efficiency
21-Mar	9:00 AM	73.58	98.44	93.99	94.41	64.27
	12:00 PM	74.74	98.59	99.93	95.03	69.97
	3:00 PM	73.84	98.5	96.69	94.57	66.50
21-Jun	9:00 AM	76.38	98.66	99.49	95.05	71.26
	12:00 PM	78.07	98.76	100	95.44	73.58
	3:00 PM	76.54	98.66	99.63	95.09	71.54
23-Sep	9:00 AM	73.71	98.47	96.06	94.5	65.88
	12:00 PM	74.63	98.59	99.92	95.01	69.85
	3:00 PM	73.57	98.44	94.62	94.42	64.70
22-Dec	9:00 AM	67.44	97.5	87.05	93.45	53.48
	12:00 PM	67.81	97.95	97.05	94.24	60.74
	3:00 PM	67.12	97.58	84.11	93.4	51.45

### 6.9 Optical Efficiency analysis of two sites

Both the sites being in the same location receive almost the same amount of solar irradiation. Therefore, it is understandable that trend for optical efficiency remains similar for both the sites. Although depicting the real surfaces introduced some dissimilarities between these sites, which ultimately resulted in a variation in Optical Efficiency presented in Figure 6.12. Because of the position and alignment of layout of Site 1 it is prominent in resulting a bit higher optical efficiency at any instance.

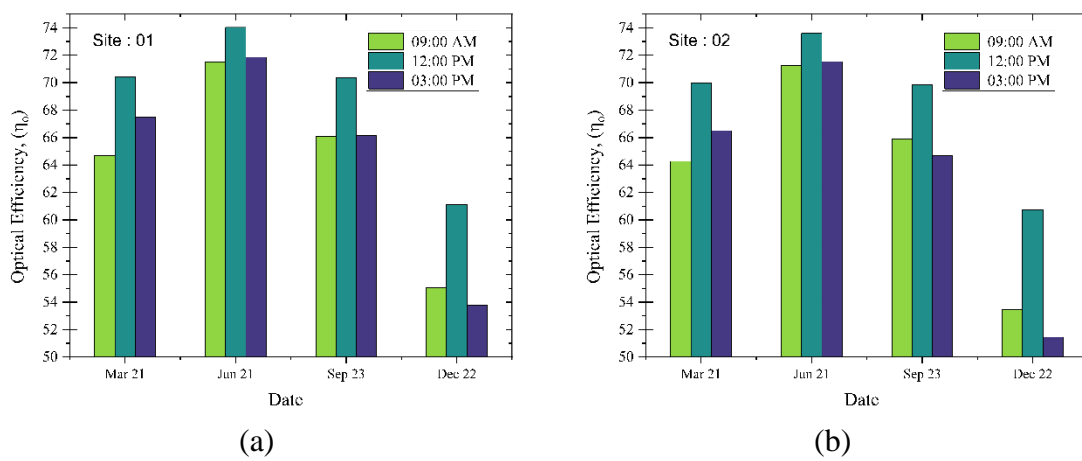


Figure 6. 12. Optical efficiency throughout the year for selected sites.

### **6.10 Overall potential of the sites**

Given that both the sites result in optical efficiency ranging from 51% to 74% they are very suitable for an H-CSP project. Initial land cost being very reasonable these two sites challenge only the installation and maintenance process of heliostats. Since site 2 has a lesser inclination on both wings it might be easier and less costly to install and maintain heliostats on the plant. A LCOE (Levelized Cost of Electricity) can be conducted to choose the reasonable one from the two.

## **Conclusion**

### **7.1 Concluding remarks**

To investigate the inclined V-shape layout mimicking the hillside inclined surfaces in terms of optical efficiency at three locations of United States in this study. A major intention behind this is to utilize the rocky or non-green hill areas. The V-shape layout was generated and simulated for cosine, shadowing, blocking and intercept efficiencies, thus Optical efficiency in SolarPILOT. The results from the simulations show that the optical efficiency is slightly higher than the currently functioning Crescent Dunes solar thermal powerplant, regardless of the fact that crescent dunes is at Tonopah, Nevada and the locations chosen in this study based on irradiation as well as less green hill areas are different.

- a. However, as the flat layout of the Cresent Dunes cannot be utilized in the hilly areas, present study has to be conducted with a feasible inclined layout. Alongside, the V-shape layout can provide a high optical efficiency in the morning and afternoon of a day. This is because of the higher cosine efficiency of the layout in the morning and at noon.
- b. Based on the overall optical efficiency and other factors like DNI, average elevation, inclination of the hill surfaces of the three locations Blue canyon has been selected to investigate further to find out some real potential site locations. Google Earth data was the source to search for the sites on this occasion.
- c. The site locations being selected, the study further required the coordinates of the real surfaces and the optimum layout to be generated. 17 test layouts have been tested for site 1 and 9 test layouts have been tested for site 2. Some of the generated test layouts were performing really well but seemed impractical to implement. After this thorough research two layouts for the two sites were found to be performing good with practical senses.

## Chapter 7

- d. Therefore, another investigation on optical efficiency has been made on these two sites and revealing that despite Site 2 having a bit less optical efficiency than Site 1, it has much potential to be utilized as a H-CSP plant.

### **7.2 Limitations and future work**

This research has been conducted with utmost care and rigorous effort. Regardless, the authors do not have the ability to conduct every possible scenario. Generation of new codes and layouts for the inclined surfaces and locating new sites both physically and virtually through platforms like Google Earth can be a scope of further study. Meanwhile the study concentrates on the barren hill tracks to be utilized, Therefore, not all hill tracks are subject of the study, rather those which has lesser green, high solar irradiation, and an average inclination between  $7^{\circ}$  to  $30^{\circ}$  are the points of interest. Also, since the central receiver has intensified solar flux intensity at some specific directions, TES design can be a subject to study further to extract the maximum amount of heat from the receiver. Further research must be conducted to evaluate the conclusions and to endorse the proposal and agreements proposed by the authors.

## References

- [1] J. Selvaraj and N. A. Rahim, “Multilevel Inverter For Grid-Connected PV System Employing Digital PI Controller,” *IEEE Transactions on Industrial Electronics*, vol. 56, no. 1, pp. 149–158, 2009, doi: 10.1109/TIE.2008.928116.
- [2] “Concentrating Solar-Thermal Power,” *Energy.gov*. [Online]. Available: <https://www.energy.gov/eere/solar/concentrating-solar-thermal-power>
- [3] “Concentrating Solar Power Projects NREL.” [Online]. Available: <https://solarpaces.nrel.gov/>
- [4] “Crescent Dunes concentrating solar plant begins producing electricity.” [Online]. Available: <https://www.eia.gov/todayinenergy/detail.php?id=25212>
- [5] C. J. Noone, M. Torrilhon, and A. Mitsos, “Heliostat field optimization: A new computationally efficient model and biomimetic layout,” *Solar Energy*, vol. 86, no. 2, pp. 792–803, Feb. 2012, doi: 10.1016/j.solener.2011.12.007.
- [6] H. Müller-Steinhagen and Franz Trieb, “(PDF) Concentrating solar power, - A review of the technology,” Ingenia. Accessed: Jan. 24, 2024. [Online]. Available: [https://www.researchgate.net/publication/224797493\\_Concentrating\\_solar\\_power\\_-\\_A\\_review\\_of\\_the\\_technology](https://www.researchgate.net/publication/224797493_Concentrating_solar_power_-_A_review_of_the_technology)
- [7] N. Belyakov, “Solar energy,” *Sustainable Power Generation*, pp. 417–438, Jan. 2019, doi: 10.1016/B978-0-12-817012-0.00031-1.
- [8] B. G. Miller, “Emerging Technologies for Reduced Carbon Footprint,” *Clean Coal Engineering Technology*, pp. 669–689, Jan. 2017, doi: 10.1016/B978-0-12-811365-3.00014-4.
- [9] B. Belgasim, Y. Aldali, M. J. R. Abdunnabi, G. Hashem, and K. Hossin, “The potential of concentrating solar power (CSP) for electricity generation in Libya,” *Renewable and Sustainable Energy Reviews*, vol. 90. Elsevier Ltd, pp. 1–15, Jul. 01, 2018. doi: 10.1016/j.rser.2018.03.045.

- [10] A. K. Pandey, R. K. R., and M. Samykano, “Solar energy: direct and indirect methods to harvest usable energy,” *Dye-Sensitized Solar Cells*, pp. 1–24, Jan. 2022, doi: 10.1016/B978-0-12-818206-2.00007-4.
- [11] IEA, “Technology Roadmap - Concentrating Solar Power – Analysis - IEA.” Accessed: Jan. 24, 2024. [Online]. Available: <https://www.iea.org/reports/technology-roadmap-concentrating-solar-power>
- [12] M. Wagner, “SolarPILOT Users Manual,” 2015.
- [13] W. B. Stine and M. A. Geyer, “Power From The Sun,” *Library of Congress, Washington, D.C. 20540 USA*, 2001, Accessed: Jan. 24, 2024. [Online]. Available: <https://www.loc.gov/item/lcwaN0004585/>
- [14] M. Schmitz, P. Schwarzbözl, R. Buck, and R. Pitz-Paal, “Assessment of the potential improvement due to multiple apertures in central receiver systems with secondary concentrators,” *Solar Energy*, vol. 80, no. 1, pp. 111–120, Jan. 2006, doi: 10.1016/J.SOLENER.2005.02.012.
- [15] M. Imran Khan, F. Asfand, and S. G. Al-Ghamdi, “Progress in research and technological advancements of commercial concentrated solar thermal power plants,” *Solar Energy*, vol. 249, pp. 183–226, Jan. 2023, doi: 10.1016/J.SOLENER.2022.10.041.
- [16] A. G. Fernández, J. Gomez-Vidal, E. Oró, A. Kruizenga, A. Solé, and L. F. Cabeza, “Mainstreaming commercial CSP systems: A technology review,” *Renew Energy*, vol. 140, pp. 152–176, Sep. 2019, doi: 10.1016/J.RENENE.2019.03.049.
- [17] M. Schmitz, P. Schwarzbözl, R. Buck, and R. Pitz-Paal, “Assessment of the potential improvement due to multiple apertures in central receiver systems with secondary concentrators,” *Solar Energy*, vol. 80, no. 1, pp. 111–120, Jan. 2006, doi: 10.1016/j.solener.2005.02.012.
- [18] M. J. Wagner and T. Wendelin, “SolarPILOT: A power tower solar field layout and characterization tool,” *Solar Energy*, vol. 171, pp. 185–196, Sep. 2018, doi: 10.1016/j.solener.2018.06.063.
- [19] O. Behar, A. Khellaf, and K. Mohammedi, “A review of studies on central receiver solar thermal power plants,” *Renewable and Sustainable Energy Reviews*, vol. 23, pp. 12–39, 2013, doi: 10.1016/j.rser.2013.02.017.

- [20] F. W. Lipps and L. L. Vant-Hull, “A cellwise method for the optimization of large central receiver systems,” *Solar Energy*, vol. 20, no. 6, pp. 505–516, Jan. 1978, doi: 10.1016/0038-092X(78)90067-1.
- [21] M. Gadalla and M. Saghafifar, “Thermo-economic and comparative analyses of two recently proposed optimization approaches for circular heliostat fields: Campo radial-staggered and biomimetic spiral,” *Solar Energy*, vol. 136, pp. 197–209, Oct. 2016, doi: 10.1016/J.SOLENER.2016.07.006.
- [22] M. Zhang, X. Du, L. Yang, C. Xu, and Y. Yang, “Comparing Study of Biomimetic Spiral and Radial Staggered Layouts of the Heliostat Field,” *Energy Procedia*, vol. 69, pp. 242–249, May 2015, doi: 10.1016/J.EGYPRO.2015.03.028.
- [23] A. Mutuberria, J. Pascual, M. V. Guisado, and F. Mallor, “Comparison of Heliostat Field Layout Design Methodologies and Impact on Power Plant Efficiency,” *Energy Procedia*, vol. 69, pp. 1360–1370, May 2015, doi: 10.1016/J.EGYPRO.2015.03.135.
- [24] A. K. M. Ashikuzzaman and S. Adnan, “Optical efficiency comparison of circular heliostat fields: Engender of hybrid layouts,” *Renew Energy*, vol. 178, pp. 506–519, Nov. 2021, doi: 10.1016/j.renene.2021.06.083.
- [25] T. W. J. Pacio, “Assessment of liquid metal technology status and research paths for their use as efficient heat transfer fluids in solar central receiver systems,” *Solar Energy*, vol. 93, p. 11-22, 2013.
- [26] J. G. Cordaro, N. C. Rubin, and R. W. Bradshaw, “Multicomponent molten salt mixtures based on nitrate/nitrite anions,” *Journal of Solar Energy Engineering, Transactions of the ASME*, vol. 133, no. 1, 2011, doi: 10.1115/1.4003418.
- [27] Q. Peng, J. Ding, X. Wei, J. Yang, and X. Yang, “The preparation and properties of multi-component molten salts,” *Appl Energy*, vol. 87, no. 9, pp. 2812–2817, 2010, Accessed: Jan. 24, 2024. [Online]. Available: <https://ideas.repec.org/a/eee/appene/v87y2010i9p2812-2817.html>
- [28] M. Kiera, “Beschreibung und Handhabung des Programmsystems HFLCAL,” *Interatom Report*, 1986.
- [29] M Izygon, P Armstrong, C Nilsson, and N Vu, “TieSOL – a GPU-based suite of softwate for central receiver solar power plants,” *SolarPACES*, 2011.

- [30] P. L. Leary and J. D. Hankins, “User’s guide for MIRVAL: a computer code for comparing designs of heliostat-receiver optics for central receiver solar power plants,” *OSTI.GOV*, 1979.
- [31] B. Belhomme, R. Pitz-Paal, P. Schwarzbözl, and S. Ulmer, “A new fast ray tracing tool for high-precision simulation of heliostat fields,” *Journal of Solar Energy Engineering, Transactions of the ASME*, vol. 131, no. 3, pp. 0310021–0310028, Aug. 2009, doi: 10.1115/1.3139139/419158.
- [32] N. Blair *et al.*, “System Advisor Model (SAM) General Description (Version 2017.9.5),” May 2018, doi: 10.2172/1440404.
- [33] P. O. of the E. Union, “SOLGATE, solar hybrid gas turbine electric power system.,” May 2005, Accessed: Jan. 24, 2024. [Online]. Available: <https://op.europa.eu/en/publication-detail/-/publication/e4f88dd1-74ac-4416-aba0-3868cc8ea5ca>
- [34] “Energy Economics: Growth, Resources and Policies - Richard John Eden - Google Books.” [Online]. Available: [https://books.google.com.bd/books?hl=en&lr=&id=Dyc4AAAAIAAJ&oi=fnd&pg=PR11&dq=Energy+Economics:+Growth,+Resources,+and+Policies&ots=H2heaE5Bfr&sig=5LUWfZuTJw9kwN\\_ddoQtyokZwC0&redir\\_esc=y#v=onepage&q=Energy%20Economics%3A%20Growth%2C%20Resources%2C%20and%20Policies&f=false](https://books.google.com.bd/books?hl=en&lr=&id=Dyc4AAAAIAAJ&oi=fnd&pg=PR11&dq=Energy+Economics:+Growth,+Resources,+and+Policies&ots=H2heaE5Bfr&sig=5LUWfZuTJw9kwN_ddoQtyokZwC0&redir_esc=y#v=onepage&q=Energy%20Economics%3A%20Growth%2C%20Resources%2C%20and%20Policies&f=false)
- [35] C. J. Noone, A. Ghobeity, A. H. Slocum, G. Tzamtzis, and A. Mitsos, “Site selection for hillside central receiver solar thermal plants,” *Solar Energy*, vol. 85, no. 5, pp. 839–848, May 2011, doi: 10.1016/j.solener.2011.01.017.
- [36] “Solar resource maps of USA.” [Online]. Available: <https://solargis.com/maps-and-gis-data/download/usa>
- [37] M. D. Walzel, F. W. Lipps, and L. L. Vant-Hull, “A SOLAR FLUX DENSITY CALCULATION FOR A SOLAR TOWER CONCENTRATOR USING A TWO-DIMENSIONAL HERMITE FUNCTION EXPANSION’~,” Pergamon Press, 1977.
- [38] “Crescent Dunes Solar Energy Project Concentrating Solar Power Projects NREL.” [Online]. Available: <https://solarpaces.nrel.gov/project/crescent-dunes-solar-energy-project>